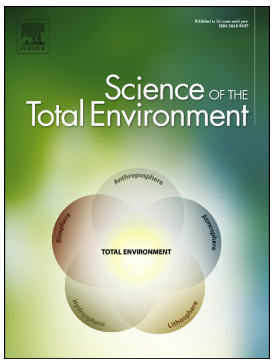

Tidal induced dynamics and geochemical reactions of trace metals (Fe, Mn, and Sr) in the salinity transition zone of an intertidal aquifer

Yi Liu, Christelle Not, Jiu Jimmy Jiao, Wenzhao Liang, Meiqing Lu

PII: S0048-9697(19)30234-7
DOI: https://doi.org/10.1016/j.scitotenv.2019.01.374
Reference: STOTEN 30688

To appear in: *Science of the Total Environment*

Received date: 16 November 2018
Revised date: 16 January 2019
Accepted date: 16 January 2019

Please cite this article as: Y. Liu, C. Not, J.J. Jiao, et al., Tidal induced dynamics and geochemical reactions of trace metals (Fe, Mn, and Sr) in the salinity transition zone of an intertidal aquifer, Science of the Total Environment, https://doi.org/10.1016/j.scitotenv.2019.01.374

Tidal induced dynamics and geochemical reactions of trace metals (Fe, Mn, and Sr) in the salinity transition zone of an intertidal aquifer

Yi Liu[1,2], Christelle Not[1,3], Jiu Jimmy Jiao[1,2,*], Wenzhao Liang[1,2], Meiqing Lu[1]

[1] *Department of Earth Sciences, The University of Hong Kong, Pokfulam Road, Hong Kong, China. Telephone: +852 2857-8246, E-mails: yiliuyl@hku.hk, jjiao@hku.hk,*

[2] *Shenzhen Research Institute, The University of Hong Kong, Shenzhen, China*

[3] *The Swire Institute for Marine Science, The University of Hong Kong, Cap d'Aguilar, Hong Kong, China.*

[*] *Corresponding author*

Abstract

Biogeochemical reactions in an intertidal aquifer influences the submarine groundwater discharge (SGD) associated trace metal flux to the ocean. Tidal fluctuation greatly affects the physical mixing, and biogeochemical transformation of trace metals in the intertidal aquifer. This study presents the dynamics of trace metals (Fe, Mn, and Sr) and the production of Fe^{2+} in the salinity transition zone is discovered. The variations of Fe^{2+} are led by the shifts of both physical mixing and biogeochemical reaction during tidal fluctuation. The transformation from amorphous $Fe(OH)_3$ to FeS is the main reason for the enrichment of Fe^{2+} in the zone with a salinity of 0.5 ~ 10. Mn behaves much less active than Fe in the intertidal aquifer due to the very limited Mn in the solid phase and the major driving force of Mn^{2+} variation is the physical mixing rather than geochemical reaction. Sr^{2+} behaves conservatively and shows a synchronous with salinity in the salinity transition zone. This study found that Fe^{2+} precipitates in a form not limited to Fe (hydro)oxides and the FeS minerals is the most possible form of precipitation in reduced aquifers. In that case, only a small part of Fe^{2+} discharges to the sea associated with SGD, but Mn^{2+} has a comparatively conservative property during the transport in the intertidal aquifer and majority of the Mn^{2+} originated from fresh groundwater will discharge with SGD in this study. The biogeochemical transformation pathways of Fe and Mn observed in this study provides insights into the cycles of Fe and Mn in an intertidal aquifer, which is of significance to accurately estimate the SGD derived Fe and Mn fluxes to the ocean.

Keywords: Iron (Fe), Manganese (Mn), Strontium (Sr), Salinity transition zone, Biogeochemical reactions, Tidal fluctuation, Submarine groundwater discharge (SGD)

1 Introduction

Submarine groundwater discharge (SGD) has been recognized as an important pathway for the discharge of carbons, nutrients, trace metals, and other dissolved species to oceans (Johannesson et al., 2011; Kroeger et al., 2007; Liu et al., 2014; Porubsky et al., 2014; Rodellas et al., 2015; Santos et al., 2008; Slomp and Van Cappellen, 2004; Trezzi et al., 2016; Windom et al., 2006). Geochemical reactions in coastal aquifers significantly affect the trace metal loadings via SGD and subsequently have great impacts on oceanic environment and ecology (Beck et al., 2007; Beck et al., 2008; Shaw et al., 1990). The intertidal aquifer, as a transition zone between the terrestrial and oceanic environments, has intensive biogeochemical reactions and frequent exchanges between liquid and solid phases (Moore, 1999). In addition, the intertidal aquifer is greatly influenced by semi-diurnal or diurnal tidal fluctuation, spring-neap tidal oscillation, wave setup, hurricane, and seasonal hydrologic variation (Heiss and Michael, 2014; Liu et al., 2016; Robinson et al., 2007; Xin et al., 2010). The dramatic shift of hydrodynamics and redox condition induced by these variations alters biogeochemical reactions in the intertidal aquifer and subsequently influences the chemical composition of SGD fluxes (Heiss et al., 2017).

Iron (Fe) and manganese (Mn) with abundances of 5.6×10^4 and 9.5×10^2 ppm, respectively, are the first and third most abundant transition metals in the earth crust (Martin, 2005). Fe and Mn play crucial roles in photosynthesis processes of phytoplankton in seawater and also serve as essential micronutrients for marine microorganisms (Holloway et al., 2016; Tagliabue et al., 2017). Redox transformations of Fe(II and III) and Mn(II, III, and IV) considerably alter dissolved Fe and Mn in coastal groundwater and have received numerous attentions world widely (Beck et al., 2009; Charette and Sholkovitz, 2002; Dulaiova et al., 2009; Holloway et al., 2016; Roy et al., 2011; Sanders et al., 2012; Snyder et al., 2004). For example, at Waquoit Bay, the groundwater-borne dissolved ferrous iron was oxidized by the dissolved oxygen in circulated seawater (Charette and Sholkovitz, 2002). Then, the ferrous iron precipitated as forms of ferrihydrite, lepidocrocite, and goethite on the surface coating of sediments in the intertidal aquifer. The intertidal aquifer acts as a geochemical barrier for iron and other elements that are highly adsorptive to iron oxides such as phosphorus, thorium, and arsenic (Beck et al., 2010; Bone et al., 2006; Charette et al., 2005; Spiteri et al., 2008). Manganese oxides have a stronger affinity than iron oxides to elements such as barium and radium. (Beck et al., 2010; Charette and Sholkovitz, 2006; Charette et al., 2005). In addition, the reduction of manganese and iron oxides plays an noteworthy role in remineralization of organic carbon catalyzed by

microorganisms in the intertidal aquifer (Roy et al., 2011). The reduction of manganese oxides releases more free energy than that of iron oxides. Therefore, in suboxic/anoxic and low nitrate environments the electron transfer catalyzed by microorganisms from electron donors such as organic matters, methane, and sulfide to high valence Mn (III and IV) is easier than that to Fe(III) (Schulz and Zabel, 2006). Manganese and iron in groundwater are more likely to be reduced and exist in low valence owing to the existence of reducers such as organic carbon and hydrogen sulfide in the intertidal aquifer. However, the low valence ferrous iron may precipitate in forms of pyrite (FeS_2) and iron sulfide (FeS) in the intertidal aquifer (McAllister et al., 2015). The hydrogen sulfide (H_2S), as a product of sulfate reduction, is transported to iron oxides zone through advection or molecular diffusion, and reacts with iron oxides to produce iron sulfide (FeS) minerals in the intertidal aquifer (McAllister et al., 2015; Snyder et al., 2004). As a consequence, iron in low valence is also active in the intertidal aquifer. Complex transformation between Fe(II) and Fe(III) occurs in the intertidal aquifer. As an alkaline earth metal, strontium (Sr) is found to be stable in the intertidal aquifer (Beck et al., 2013; Gonneea et al., 2014; Rahaman and Singh, 2012; Trezzi et al., 2017), even though Sr isotope exchange induced by geochemical reactions is common (Beck et al., 2013; Charette and Sholkovitz, 2006). Therefore, Sr can be used as an indicator for physical mixing induced by infiltration of seawater and subsequently used to evaluate the variation of Fe and Mn led by biogeochemical reactions in the intertidal aquifer.

Various factors influence the dissolution and precipitation of iron minerals. For example, pH is a major controlling factor in the oxidative precipitation of ferrous iron (Beck et al., 2010; Spiteri et al., 2006). Iron precipitation is found to be favorable in the freshwater/seawater mixing zone with a pH between 5.5 to 7.9 (Spiteri et al., 2006). In addition, the seasonal variation of Mn and Fe in the upper decimeter of tidal flats is found to be sensitive to the organic carbon supply, redox stratification, and atmospheric particulate matters (Beck et al., 2008). A decline of diagenesis rate of iron oxides and organic matters is led by a decrease of fresh SGD flux (Roy et al., 2013). Other factors such as the microbial communities (Sulu-Gambari et al., 2016) and sea level rise (Roy et al., 2010) are also reported to have great impacts on the oxidation and reduction of iron and manganese. Tidal pumping is a major driving force for the land-sea water and material exchange. The composition of groundwater in the intertidal aquifer will be altered by the physical mixing and chemical reaction with the infiltrated seawater induced by tidal pumping (Liu et al., 2017c). Furthermore, tidal fluctuation modifies the land-sea hydraulic gradient, which results in the oscillation of seawater-freshwater transition zone (Heiss and Michael, 2014). The redox condition in the transition

zone was also found to change with the tidal fluctuation (Liu et al., 2018b). Therefore, geochemical reactions in the intertidal aquifer are hypothesized to vary significantly at different tidal stages, and alters the concentration and spatial distribution of Fe and Mn but has no influence on that of Sr. To test this hypothesis, a field study was conducted at a sandy beach of Tolo Harbor, Hong Kong. Groundwater samples from different lateral and vertical locations of the salinity transition zone of an intertidal aquifer were collected every three or four hours within two tidal cycles (48 hours) to investigate the spatial distribution and temporal variation of dissolved Fe, Mn, and Sr in response to tidal fluctuation. Based on dynamics of dissolved trace metals, the concentration of solid phase of trace metals, and the mineralogy of sediments, the geochemical reactions in the intertidal aquifer are better investigated and the hypothesis of tidal fluctuation impacts on these geochemical reactions is examined.

2 Material and Method

2.1 Study site

Tolo Harbor is a semi-closed embayment at the northeast of New Territories, Hong Kong (Figure 1a). The Harbor has a limited water exchange with open sea due to its bottle necked configuration and prevailing northwesterly wind direction (Lee et al., 2012). The basic topography, hydrology, and meteorology conditions of Tolo Harbor can be found in previous studies of this area (Lee et al., 2012; Luo and Jiao, 2016; Luo et al., 2014; Tse and Jiao, 2008). The sampling site (22˚ 28' 06.91" N, 114˚ 13' 02.22" E) is located at a sandy beach of Tolo Harbor (Figure 1a). A permanent multilevel sampling system (Luo et al., 2017) was installed within the intertidal aquifer (Figure 1b). The sampling system contains 11 sampling sites but only 3 of them located within the salinity transition zone were used in this study (L1, L2, and L3 in Figure 1b). The detailed setup of the sampling cross section can be found in Liu et al. (2017b). The hydraulic conductivity of the shallow intertidal aquifer is measured to be 4.57 m/d through falling head permeability test at the beach (Liu et al., 2018a). The sediment samples were collected on the sandy beach for grain size analysis and porosity measurement in laboratory. The sediments were classified as well graded gravelly sands according to the Unified Soil Classification System and the porosity was measured to be ~ 0.3 in the laboratory (Liu et al., 2018a) following the standard procedure (Fetter, 2000). The semi-diurnal tide in Tolo Harbor has an average tidal range of ~ 1.06 m and a mean sea level of ~ 1.45 mPD (meter above principal datum). The time series of tidal level was recorded by an automatic monitoring transducer (Cera-Diver, Schlumberger Water Service) installed in

the harbor ~120 m from the mean tidal mark along the sampling transect (D4 in Figure 1b). In addition, another monitoring well was installed near L2 to record the groundwater level (D2 in Figure 1b).

2.2 Water sample collection and analysis

Fifteen rounds of groundwater sampling were conducted between 23rd and 25th, May, 2016. The groundwater was extracted from sampling tubes in the salinity transition zone except L1-1 and L3-2 (white dots shown in Figure 1b) due to the slow pumping rate. At each sampling site, all sampling tubes were connected to different peristaltic pumps and the groundwater at different depths was extracted at the same time to minimize the disturbance induced by vertical flow. During each sampling round (called SR hereafter), nine groundwater (GW) samples with a volume of 0.5 ~ 1 L for each and one nearshore seawater (called NSW hereafter) sample with a volume of 4 L were collected. The tidal level and sampling time during each SR are presented in Figure 2. During SRs 06, 07, 13, and 14 (marked with red color in Figure 2), the tidal level is higher than the beach surfaces of L2 and L3. During other SRs (marked with green color in Figure 2), the tidal level is lower than the beach surfaces of L2 and L3. L1 is not submerged by seawater throughout the sampling period. The groundwater physicochemical parameters such as salinity, pH, dissolved oxygen (DO) and oxidation/reduction potential (ORP) were measured *in-situ* with a portable multi-parameter meter (HI 98194, Hanna Instruments) immediately after the sample collection. The resolution and accuracy of salinity, DO, ORP, and pH are 0.01 and ±0.01, 0.01 and ±0.10 ppm, 0.1 and ±1.0 mV, and 0.01 and ±0.02 pH, respectively. During the 15 SRs in the sampling period (48 hours), 150 samples (GW and NSW) in total were collected for analysis of dissolved trace metals (Fe, Mn, and Sr). The water sample was filtered with 0.45 μm syringe filter first. Then the water sample was acidified with 16 N HNO_3 solution to establish a pH below 2. The acidified sample was preserved in an ice box during the sampling period and stored in refrigeration environments (4 ˚C) in laboratory. The trace metals analyses were carried out with an Inductively Coupled Plasma Optical Emission Spectrometer (ICP-OES) in Central Facilities at School of Biological Science, the University of Hong Kong. The GW and NSW samples were pre-diluted 10 times with 2% HNO_3 solution. Seven-point calibration was conducted with a multi-element calibration standard (Perkin Elmer Pure, Trace Metal III, #N9300213). During sample analysis, one reference standard (Perkin Elmer Pure, Trace Metal I, #N9300211) with known concentration of each element was measured after every ten sample to evaluate the stability of ICP-OES. The accuracy and precision are better than 4.7%, and 4.8% for Fe, 7.9%, and 2.1% for Mn, and 5% and 4.5% for Sr, respectively.

2.3 Sediment sample collection and analysis

A sediment core (Core 1) was collected near sampling site L2 while another sediment core (Core 2) was collected at L4 (Figure 1). The sediment core was separated into slices with 2 cm interval and the slices were stored in sample bags separately. Then, the sediment sample was freeze-dried in vacuum before analysis. The sediment sample was mounted on glass slide and coasted with gold, and then was scanned and pictured by a field emission scanning electron microscope (SEM) (Hitachi S-4800) at the Pathology Department of Queen Mary Hospital, the University of Hong Kong. Duplicate sediment sample was digested in graphite digestion instrument (EHD-36-iTouch, Lab Tech) for the measurement of solid phase Fe, Mn, and Sr. Specifically, 0.5 g sediments with grain size smaller than 500 μm was weighted and placed in the polytetrafluoroethylene (PTFE) tube. Then, 5 ml 65% HNO_3 solution, 3 ml 40% HF solution, and 2 ml 70% $HClO_4$ solution were added into PTEF tube for sediments digestion. The PTEF tube was sealed and shook for 1 min, followed by heated to 120 ˚C and kept for 30 min. After that the PTEF tube was heated to 150 ˚C and kept for 2 hours. Then, unscrew the PTEF tube and raise the temperature to 190 ˚C until 1 ml solution was remained. Lastly, dilute the digested sample to 50 ml with deionized water for measurement. The prepared samples for solid phase of trace metals were measured via an Inductively Coupled Plasma Mass Spectrometry (ICP-MS) at the Southern University of Science and Technology. The precision is better than 1% for all trace metals while the accuracy is better than 1.7 % for Fe, 1.6% for Mn, and 2.4% for Sr.

3 Results

3.1 Redox conditions and water mass

According to the salinity and composition of stable isotopes (δ^2H and $\delta^{18}O$), the groundwater in the salinity transition zone is separated into three different groundwater masses, i.e., shallow fresh groundwater (shallow FGW) (L1-2) with salinity < 0.5, δ^2H > -30‰, and $\delta^{18}O$ > -5.1‰, deep FGW (L2-4) with salinity < 0.5, δ^2H < -30‰, and δ $\delta^{18}O$ < -5.1‰, and saline groundwater (L2-1 to L2-3, L3-1 to L3-5) with salinity > 0.5 (Liu et al., 2017c). The redox conditions in the three groundwater masses of groundwater are very distinct to each other (Liu et al., 2018c). According to Table 1, the shallow FGW has a higher content of DO than the other two water masses and the saline groundwater has a higher pH and salinity due to the mixing NSW with high salinity (24.49) and pH (8.21). The deep FGW is slightly oxic due to the existence of higher content of NO_3^- than other two water masses as indicated in Liu et al. (2017c) and (Liu et al., 2018d). The saline groundwater with average ORP of -107.7 mV is much more reduced

than its mixing endmembers, shallow FGW (-30.5 mV), deep FGW (12.20 mV), and NSW (-55.30 mV), indicating that the geochemical reactions tend to decline the ORP of saline groundwater in the salinity transition zone of intertidal aquifer.

3.2 Dissolved strontium (Sr)

In shallow FGW, Sr^{2+} ranges from 0.05 to 0.14 mg/L with an average value of 0.09 mg/L (Table 1). Shallow FGW has a Sr^{2+} concentration slightly higher than deep FGW (0.09 versus 0.05 mg/L) while NSW has a Sr^{2+} concentration much higher than deep FGW (3.55 versus 0.05 mg/L). As the mixture of the three endmembers (shallow FGW, deep FGW, and NSW), saline groundwater has a large range of Sr^{2+} (0.10 ~ 3.30 mg/L) due to the different degree of mixing. The average Sr^{2+} concentration in saline groundwater is 1.00 mg/L. The detailed Sr^{2+} concentration of each groundwater or seawater sample can be found in Table S1.

Owing to the conservative behavior of Sr^{2+} in intertidal aquifer, the spatial distribution and temporal variation of Sr^{2+} (color in Figure 3) is very similar to that of salinity (solid line in Figure 3). During high tide (SR 06, 07, 13, and 14), NSW submerges the beach surface at L2 and L3 resulting in an obvious increase of Sr^{2+} in near-surface zone at a depth of 0.5 m. For instance, the sea level increases from -0.49 m to 0.8 m during SR 12 and 13, Sr^{2+} increases from 1.48 to 3.02 and 2.00 to 2.59 mg/L at L2-1 and L3-1, respectively. During ebbing tide, Sr^{2+} decreases in saline groundwater, which is caused by a strengthened seaward advection induced by sea level drop. For example, while the tidal level decrease from 0.8 m to -0.1 m from SRs 07 to 08, Sr^{2+} decrease from 2.79 to 1.97 mg/L at L2-1, and from 2.69 to 2.12 mg/L at L3-1.

3.3 Dissolved iron (Fe)

The dynamics of dissolved Fe in the salinity transition zone is presented in Figure 4 and the Fe^{2+} in each groundwater mass and each individual water sample can be found in Table 1 and Table S1, respectively. In shallow FGW, Fe^{2+} ranges from 1.83 to 3.86 mg/L with an average value of 3.13 mg/L. Fe^{2+} in deep FGW is lower than that in shallow FGW (0.98 versus 3.13 mg/L). In NSW, Fe^{2+} (average value of 0.18 mg/L and range of 0.04 ~ 0.65 mg/L) is much lower than that in the two fresh water masses (shallow and deep FGW). Fe^{2+} is distinct in saline groundwater from its mixing endmembers (shallow FGW, deep FGW, and NSW). In saline groundwater, Fe^{2+} varies from 0.10 to 14.43 mg/L with an average value of 4.58 mg/L. The average Fe^{2+} is much higher in saline groundwater than in deep FGW and NSW, and slightly higher than in shallow FGW. The higher Fe^{2+} in saline

groundwater than its mixing endmembers indicates the production of Fe^{2+} in this zone (salinity transition zone). The enriched Fe^{2+} in saline groundwater could be resulted from the reduction of iron oxides or the dissolution of iron minerals (FeS and FeS_2). Therefore, the source of Fe flux to the ocean may be from the shallow FGW and produced locally via dissolution of iron minerals.

Spatially, owing to the infiltration of low Fe^{2+} NSW, Fe^{2+} is very low (1.42 mg/L for L2-1 and 0.41 mg/L for L3-1) in near-surface zone (L2-1 and L3-1) with a depth of ~ 0.5 m. Additionally, there is a high Fe^{2+} zone (L2-2, L2-3, L3-3, and L3-4) located in the transition zone with a salinity of 0.5 ~ 10 (Figure 4), in which Fe^{2+} ranges from 2.24 to 14.43 mg/L with an average value of 6.50 mg/L. The maximum Fe^{2+} is observed at L3-4 with a depth of 1.8 m. In near-surface zone, 2 to 6.5 times dilution of Fe^{2+} is observed after infiltration of NSW (Figure 4). Fe^{2+} at L3-5 is not as high as L3-4 with a value of 4.23 mg/L. According to Figure 4, a decreasing trend of Fe^{2+} in the transition zone with a salinity of 0.5 ~ 10 g/kg can be observed during flooding tide whereas an increasing trend is observed during ebbing tide. For example, Fe^{2+} in the transition zone declines from SRs 02 to 04 but raises from SRs 14 to 15. This might be due to the lacks of electron supplier from FGW from inland area during SRs 02 & 04 to release Fe^{2+} from Fe oxides in the salinity transition zone whereas the landward flow of saline groundwater during high tide (SR 14) brings reducers such as H_2S and organic carbon to release Fe^{2+} from Fe oxides since saline groundwater has a higher H_2S and organic carbon than the fresh groundwater from inland area.

3.4 Dissolved manganese (Mn)

The spatial distributions of Mn^{2+} at different tidal stages are illustrated in Figure 5. The Mn^{2+} in each water mass and individual sample is listed in Table 1 and Table S1, respectively. Mn^{2+} is about one order of magnitude smaller than Fe^{2+} in each groundwater mass. Specifically, in opposition to the fact that deep FGW has a much lower Fe^{2+} concentration than shallow FGW (0.98 versus 3.13 mg/L), the concentration of Mn^{2+} in deep FGW is comparable to that in shallow FGW (0.25 versus 0.29 mg/L). Mn^{2+} in NSW, ranging from 0.0001 to 0.04 mg/L with an average value of 0.003 mg/L, is much lower than those in the two fresh water masses. Compared to shallow and deep FGWs, saline groundwater has a Mn^{2+} concentration with a larger range (0.06 to 0.63 mg/L) but a similar average value (0.27 mg/L).

Similar to the spatial distribution of Fe^{2+} (Figure 4), there is a zone in saline groundwater (salinity of 0.5 ~ 10; L2-2, L2-3, L3-3, and L3-4) with a very high Mn^{2+} (ranges from 0.20 to 0.63 mg/L with an average value of 0.35 mg/L).

Differently, the maxima Mn^{2+} is observed at L2 (L2-2 and L2-3) with a depth of 1 ~ 1.5 m (Figure 5) whereas the maxima Fe^{2+} is observed at L3 (L3-3 and L3-4) with a depth of 1.5 ~ 1.8 m (Figure 4). Because of the very high Mn^{2+} observed at L1-2 and even higher Mn^{2+} observed at the locations shallower than L1-2 in previous study (Liu, 2017), the major source of Mn^{2+} in the salinity transition zone is speculated to be the shallow FGW from inland rather than the reduction of Mn oxides locally. Mn^{2+} at L3-5 is very low with a value of 0.11 mg/L. The near-surface zone (L2-1 and L3-1) has a very low Mn^{2+} and suffers from the dilution of NSW, which is demonstrated by a lower Mn^{2+} at high tide (SRs 06, 07, 13, and 14) than low tide (Figure 5). The seaward movement of Mn^{2+} is strengthened by a large land-sea hydraulic gradient at low tide as demonstrated by a seaward movement of Mn^{2+} plume at low tide (from SR 01 to 02, SR 08 to SR 09, and SR 14 to 15).

3.5 Solid phase of trace metals

The solid phase of trace metals (Fe, Mn, and Sr) is illustrated in Figure 6. In core 1 (Figure 6a), Mn ranges from 20.85 to 99.16 μg/g and Sr varies from 3.46 to 31.55 μg/g (Table S2). The solid phase of Fe (4059.23 ~ 27847.90 μg/g) is two orders of magnitudes greater than Mn and Sr (Table S2). Similar to core 1, core 2 has a much higher Fe in solid phase (3765.26 ~ 55167.70 μg/g) than Mn (18.89 ~ 136.93 μg/g) and Sr (7.26 ~ 224.91 μg/g) (Figure 6b). Owing to the different flow dynamics and redox conditions (Figure 6c), the concentration and distributions in core 1 and core 2 are distinct to each other.

Horizontally, the solid phase of trace metals has a higher concentration in core 2 than core 1. Specifically, the average concentration of Mn, Fe, and Sr in core 2 is 48.77 ± 25.25, 15665.10 ± 12824.9, and 83.64 ± 76.78 μg/g, respectively, which are 1.3, 1.5, and 8.8 times that in core 1 (Table S2). Two reasons are responsible for the increase of Fe and Mn from core 1 to core 2. Firstly, core 1 collected in the mangrove zone has a higher degree of organic matter than core 2 sampled at the bare beach. As a result, the remineralization of organic matter consumes more the high valence Mn and Fe in core 1 than core 2 and results in a lower Mn and Fe in core 1 than core 2. Secondly, groundwater at core 1 has a lower pH and is more reduced than that at core 2 (Liu et al., 2018d), which means an easier reductive dissolution of Fe and Mn oxides at core 1 than core 2 (Martin, 2005). Differently, the dramatic rise of Sr from core 1 to core 2 is not linked to the redox reactions. Since the dissolved Sr is much higher at core 2 than at core 1 due to the higher groundwater salinity, a higher content of Sr in the solid phase is needed to maintain the equilibrium between the solid and dissolved Sr.

Vertically, the solid phase of Fe in core 1 (Figure 6a) gradually increases from 4059.23 μg/g at 7.5 cm to 15684.50 μg/g at 27.5 cm, which is caused by the decrease of organic matter. Followed by a decline from 5684.50 (27.5 cm) to 6110.19 μg/g (67.5 cm), the Fe in solid phase rises again to 27847.90 μg/g at 97.5 cm (Table S2). The enrichment of Fe below 67.5 cm is caused by the increase of ORP values and more Fe exists in solid phase. Mn has the similar trend with Fe whereas Sr has very small variations in the upper 92.5 cm. Sr increases from 3.76 μg/g at 92.5 cm to 31.55 μg/g at 97.5 cm, which is potentially caused by scavenging to authigenic iron oxides (Andersson et al., 1994) or adsorption of Fe-oxyhydroxides in the sediments (Beck et al., 2013; Charette and Sholkovitz, 2002). In core 2 (Figure 6b), the synchronous changes of Fe, Mn and Sr are observed. The solid phase of all trace metals is stable until a depth of 42 cm, then increases. The enrichment of Mn and Fe are caused by the precipitation of high concentration dissolved Mn and Fe in groundwater discharged from the salinity transition zone. The enrichment of Sr is caused by the enrichment of Fe and Mn since Sr may adsorbed to Fe-oxyhydroxides in the sediments as stated previously.

4 Discussions

Fe^{2+}, Mn^{2+}, and Sr^{2+} display different behaviors in the salinity transition zone. Obviously, Sr and Mn are comparatively conservative compared to Fe from the geochemical perspectives in this study. As presented previously, Fe^{2+} increase first at the freshwater front of the salinity transition zone and then decrease during the advection to ocean. However, a generally decreasing trend of Mn^{2+} and an increasing trend of Sr^{2+} from land to sea are observed (Liu, 2017). To explain the featured spatial distribution of Fe^{2+}, Mn^{2+}, and Sr^{2+}, the possible biogeochemical processes are examined in the following sections. First, the factors including the oxidation processes in the catchment and salinity transition that affects the spatial distribution of Fe^{2+} and Mn^{2+} are investigated. Then, the discussion on the variation of trace metals induced by tidal fluctuation is presented. The trace metal variations caused by biogeochemical reactions and physical mixing are distinguished and evaluated separately. After that the role of the salinity transition zone played in biogeochemical reactions of Fe^{2+} and Mn^{2+} is evaluated via the estimation of apparent production (or removal) rates of Fe^{2+} and Mn^{2+} in the salinity transition zone. Then, the geochemistry of Fe and Mn in the salinity transition zone is discussed based on the analysis in previous sections. At the end the findings of this study are generalized into a conceptual model to present the full view of geochemical

cycling of Fe and Mn in the salinity transition zone and gives implications to the discharges of Fe^{2+} and Mn^{2+} with SGD.

4.1 Factors influencing spatial distributions

4.1.1 Oxidation rates of Mn^{2+} and Fe^{2+} in FGW

Abiotic homogeneous and heterogeneous oxidations are two parallel pathways that precipitate Fe^{2+} and Mn^{2+} as Fe and Mn oxides, respectively. The abiotic homogeneous oxidation rates of Fe^{2+} and Mn^{2+} can be described as a function of pH and DO, which can be expressed as (Martin, 2005; Spiteri et al., 2006),

$$-\left(\frac{d[\mathrm{Fe^{2+}}]}{dt}\right) = (k_0[\mathrm{Fe^{2+}}] + k_1\beta_1\frac{[\mathrm{Fe^{2+}}]}{[\mathrm{H^+}]} + k_2\beta_2\frac{[\mathrm{Fe^{2+}}]}{[\mathrm{H^+}]^2})[\mathrm{O_2}], \quad (1)$$

where $k_0 = 0.029$ M^{-1} h^{-1}, $k_1 = 9.04 \times 10^4$ M^{-1} h^{-1}, $k_2 = 2.86 \times 10^{10}$ M^{-1} h^{-1} are the rate constants at a temperature of 25 ˚C. The $\beta_1 = 3.2 \times 10^{-10}$ M, $\beta_2 = 2.5 \times 10^{-21}$ M^2 are the apparent equilibrium constants, respectively.

For Mn^{2+}, the oxidation rates can also be described as a function of pH and DO (Martin, 2005):

$$-\left(\frac{d[\mathrm{Mn^{2+}}]}{dt}\right) = k_2\beta_2\frac{[\mathrm{Mn^{2+}}]}{[\mathrm{H^+}]^2}[\mathrm{O_2}], \quad (2)$$

where $k_2 = 1.80 \times 10^5$ M^{-1} h^{-1} is the rate constant at a temperature of 25 ˚C and $\beta_2 = 10^{-22}$ M^2.

Applying Eq. (1), abiotic oxidation rates of Fe^{2+} in shallow and deep FGW are calculated to be 9.13 µM h^{-1} and 0.65 µM h^{-1}, respectively. The abiotic oxidation rate of Fe^{2+} is higher in shallow FGW than in deep FGW due to a low Fe^{2+} and DO in deep FGW. Since deep FGW has a longer residence time in the aquifer than shallow FGW, more Fe^{2+} has been removed from deep FGW by the oxidation process in the aquifer before the sample collection. Although DO is much higher in shallow FGW than deep FGW (4.48 vs. 2.69 ppm), Fe^{2+} is much higher in shallow FGW than in deep FGW (3.13 vs. 0.98 mg/L). Therefore, the oxidation process in the aquifer could be either abiotic or microbially mediated Fe oxidation as suggested by McAllister et al. (2015). However, the co-existence of oxygen and Fe^{2+} in both shallow and deep FGW indicates that the Fe^{2+} removal in FGW is slow and could not be microbially mediated oxidation processes that usually have quick reaction rates. In addition, a low pH in both shallow and deep FGW leads to a slow abiotic oxidation rate according to Eq. (1), which well explains the co-existence of Fe^{2+} and oxygen in groundwater. Applying Eq. (2), the abiotic oxidation rate of Mn^{2+} in shallow and

deep FGW is 1.9×10^{-7} μM h^{-1} and 3.5×10^{-8} μM h^{-1}, respectively. The abiotic oxidation rate of Mn^{2+} is about 6 orders of magnitudes smaller than that of Fe^{2+}. As a result, the Fe^{2+} difference between shallow and deep FGW is much more significant than Mn^{2+} difference in the two water masses (2.216 vs. 0.041 mg/L).

If the concentration of Fe^{2+} in shallow FGW (3.13 mg/L) is assumed to be the initial concentration of recharged water for deep FGW and the oxidation rate of shallow FGW is used for calculation, the time for such a high Fe^{2+} (3.13 mg/L) to decrease to a low Fe^{2+} (0.98 mg/L) in deep FGW is ~ 2.5 days. However, this time is calculated under a pH around 6.50 which is significantly higher than the pH of recharge source for deep FGW (i.e., rainfall water with a pH ~ 4.5 by Fang et al. (2001)). If a pH of 4.50 is applied for calculation, the time for deep FGW to decrease from 3.13 to 0.98 mg/L is about 1113 days. Therefore, the residence time of Fe^{2+} would be expected to be 2.5 ~ 1113 days longer in deep FGW than in shallow FGW. Furthermore, if the same input of Mn^{2+} is assumed for both shallow and deep FGW, the removal of Mn^{2+} (0.041 mg/L) in deep FGW with such a small oxidation rate (1.9×10^{-7} μM h^{-1}) would take ~ 448 years, which is not consistent with the residence time difference calculated via iron differences between shallow FGW and deep FGW. Such a discrepancy between Fe and Mn is possibly caused by the significant underestimation of Mn^{2+} oxidation rate due to the neglect of Mn^{2+} oxidation catalyzed by mineral surface and by microbial communities. The Mn oxidation mediated by manganese oxidizing bacteria, such as *firmicutes*, *proteobacteria*, and *actinobacteria*, is several orders of magnitudes faster than abiotic oxidation such as homogeneous and heterogeneous oxidation of Mn (II) (Tebo et al., 2004; Tebo et al., 2005). If the time scale of Fe oxidation is assumed to be the same as Mn oxidation, the Mn oxidation rate is estimated to be $2.79 \times 10^{-5} \sim 0.012$ μM h^{-1}. Therefore, the most possible removal pathway of Fe^{2+} is abiotic homogeneous oxidation but that of Mn^{2+} is microbially catalyzed oxidation. Only Mn (II) oxidation seems to be catalyzed by the microorganism communities, which could be linked to the unique feature of Mn oxidizing bacteria. This bacteria can obtain energy for autotrophic growth by oxidizing Mn (II) (Tebo et al., 1997; Tebo et al., 2005) and also protect themselves from other environmental insults, such as UV radiation, predation, viral attack and metal toxicity, by coating with manganese oxides (Parikh and Chorover, 2005).

Eqs. (1) & (2) can also be used to calculate the homogeneous oxidation rates of Fe^{2+} and Mn^{2+} in the salinity transition zone. The oxidation rates of Fe and Mn are subsequently used to identify the potential removal forms of trace metals and corresponding form of minerals (reactants or products) participated in geochemical transformations in the aquifer in the following section.

4.1.2 The relationship of dissolved trace metal vs. salinity, pH and ORP

Fe, Mn, and Sr behave differently in response to variations of salinity, pH, and ORP. The relationships between salinity and trace metals (Fe^{2+}, Mn^{2+}, and Sr^{2+}) are presented in Figure 7. A theoretical conservative mixing between FGW and NSW endmembers is estimated and the best fit of data points is also illustrated in Figure 7.

Fe^{2+} increases with salinity at first, peaks at a salinity of 0.5 ~ 5, and then declines with salinity. The best fit of Fe^{2+} with salinity is above the theoretical conservative mixing line (TCML) indicating a production of Fe^{2+} in the salinity transition zone. Usually, Fe is more soluble in acid or reduced condition in groundwater (Hylander et al., 2000; Nath et al., 2013), and Fe precipitates rapidly with the increase of pH or ORP. However, Fe^{2+} in this study does not show an obvious correlation with pH (Figure S1a) and ORP (Figure S2a), which is probably link to geochemical reactions in the salinity transition zone that produce Fe^{2+} from iron oxides or sulfide iron and make Fe^{2+} peak at a pH of 6.7 and ORP of -100 mV.

The relationship between salinity and Mn^{2+} in the salinity transition zone is shown in Figure 7b. Similar to Fe^{2+}, Mn^{2+} increases first and then decreases with salinity. However, Mn^{2+} peaks at L2-3 rather than at L3-3 and L3-4 where Fe^{2+} peaks. It is worth noting that Mn^{2+} at L3-5 is below the theoretical conservative mixing line. This is because the groundwater at L3-5 is the mixture of deep seawater and deep FGW (Liu et al., 2018c). Since L3-5 is below L2-4 (depth: 3 vs. 2 m), the upwelling of deep FGW that mixes with L3-5 has a longer residence time and a lower Mn^{2+} than the FGW at L2-4. Generally, Mn^{2+} decreases with pH (Figure S1b) indicating that Mn is more soluble in acid condition than neutral and alkaline conditions in groundwater as observed in other studies (Atkinson et al., 2007; Hatje et al., 2003; Holloway et al., 2016). However, Mn^{2+} removal in oxic environment (ORP > 0) is not as obvious as Fe^{2+} (Figures S2b & S2a), which confirms that Mn^{2+} is much less affected by the geochemical reactions than Fe^{2+} in the system studied here. According to Figure 8, a logarithmic form of relationship between Fe^{2+} and Mn^{2+} in both FGW–upper saline plume (USP) transition zone and FGW-salt wedge (SW) transition zone Liu et al. (2018c) is observed. The increase of Mn^{2+} is hindered with the rise of Fe^{2+}, which is because the solid phase of Fe(III) is much higher than Mn(IV) and the electron suppliers such as organic matter, methane, and hydrogen sulfide would use more Fe(III) as the electron acceptor than Mn(IV).

The positive correlation between salinity and Sr^{2+} is illustrated in Figure 7c. The theoretical conservative mixing line is very close to the best fit line demonstrating that Sr^{2+} is generally conservative in the salinity transition zone of

intertidal aquifer and appropriate to serve as an indicator of physical mixing process of a cation. The values of Sr^{2+} from some sampling locations are slightly lower than the conservative mixing line (L3-3, L3-4, L2-1, and L3-1) indicating the removal of Sr^{2+} from these locations. The small discrepancy may be caused by adsorption of finer sediments in near surface zone (L3-1 and L2-1) and by adsorption of authigenic iron oxides (Andersson et al., 1994) and Fe-oxyhydroxides (Beck et al., 2013; Charette and Sholkovitz, 2002) in deep sediments with higher content of iron oxides (L3-3 and L3-4). The speculation can be confirmed by the synchronous trend of Fe and Sr in solid phase of core 1 and core 2 as shown in Figure 6. The bedrock composition in the study site is responsible for very low concentration of Sr in both shallow and deep FGW (0.087 mg/L and 0.048 mg/L) (Beck et al., 2013). Due to the physical mixing and generally conservative properties of Sr^{2+}, the saline groundwater with higher pH usually has a higher Sr^{2+} (Figure S1c). Similarly, the saline groundwater with a higher ORP usually has a higher Sr^{2+} (Figure S2c).

4.2 Tidal fluctuation induced dissolved trace metal variations

Tidal fluctuation influence on trace metals (Fe^{2+}, Mn^{2+}, and Sr^{2+}) is separated into two different aspects. Firstly, a location shift of the salinity transition zone induced by hydrodynamics oscillation represents a change of physical mixing between FGW and seawater. Salinity variation (the variation is defined as the percentage of standard deviation accounts in average value) provides information on a change of physical mixing (Table 2). However, salinity is a neutralized parameter of all ions. As so, salinity variation is expected to be smaller than the variation of a specific ion in water. Under such circumstances, a conservative ion such as Sr^{2+} (Beck et al., 2013; Gonneea et al., 2014; Rahaman and Singh, 2012; Trezzi et al., 2017) is a better choice than salinity to trace a change in physical mixing. Secondly, the oscillation of salinity, pH, DO, temperature, and ORP induced by tidal fluctuation substantially affects biogeochemical reactions such as redox reaction, cation exchange, and dissolution/precipitation of minerals (Liu et al., 2017a; O'Connor et al., 2018; O'Connor et al., 2015). Therefore, in this study Fe^{2+} (or Mn^{2+}) variation induced by geochemical reactions is estimated as a difference between Fe^{2+} (or Mn^{2+}) variation and Sr^{2+} variation.

4.2.1 Trace metal variation induced by physical mixing shift

The variation of Sr^{2+} (Table 2) is used as indicator of the physical mixing induced trace metal variation in response to tidal fluctuation in this study. The physical mixing with NSW as the major process in near-surface zone varies greatly. Because of the large contrast of Sr^{2+} in NSW and groundwater at this zone, the maximum physical mixing

variation of is observed at L2-1. The variation of Sr^{2+} at L2-1 (50.67%) is the largest among all locations in the salinity transition zone. In the zone with a salinity of 0.5 ~ 10, the physical mixing induced variation is ~ 20%. This variation is expected to be caused by a change of land-sea hydraulic gradient shift induced by tidal fluctuation. In NSW, the variation induced by physical mixing between SGD and seawater is 18.11% indicating that SGD flux varies greatly with tidal fluctuation and SGD derived chemical flux has a significant effect on chemical concentration in NSW.

4.2.2 Trace metal variation induced by geochemical reaction shift

According to Table 2, Fe^{2+} variation induced by geochemical reaction shift enlarges the total variation on the basis of variation induced by physical mixing shift. In the salinity transition zone the geochemical reaction shift induced by geochemical reaction shift ranges from 2.53% to 82.4% (Table 2). Obviously, the near-surface zone (L2-1 and L3-1) has the largest variation induced by geochemical reaction shift. As shown in Liu et al. (2017c) and Liu et al. (2018d), the production of NH_4^+ from the remineralization of organic matter is very active in this zone. The metabolism of organic matter would be expected to have great influence on the variation of Fe^{2+} since Fe oxides may participate in the geochemical reactions and serve as the electron receiver. Even though Fe^{2+} variation (2.53% ~ 29.78%) induced by geochemical reaction shift in the transition zone with a salinity of 0.5 ~ 10 (L2-2, L2-3, and L3-3 to L3-5) is not as large as the near-surface zone (31.73% ~ 53.11%), the net Fe^{2+} change (1.78 ~ 2.52 mg/L) is much larger in the transition zone than the near-surface zone due to a higher Fe^{2+} concentration in this zone. According to Eq. (1) in previous section, the abiotic oxidation rate of Fe^{2+} in the transition zone is 2.07 ~ 35.9 μM/h. Under such abiotic oxidation rates, the net change of Fe^{2+} with a concentration of 2.52 mg/L (maximum net variation of Fe^{2+}) during the sampling period only takes 4.8 ~ 21.8 h, which is well within the tidal fluctuation period (24 h). This demonstrates that the net change of Fe^{2+} in this study site can be achieved by abiotic oxidation of Fe^{2+} only as stated previously. However, to obtain a fast reduction rate, the assistance of iron reducing bacteria is necessary because abiotic reduction of iron is slow and limited by the solubility of iron oxides (Bonneville et al., 2004; Hyacinthe et al., 2006). The geochemical reaction induced Fe variation is comparable to that induced by physical mixing (Table 2), indicating the significant role of geochemical reaction in the variation of Fe^{2+} in the salinity transition zone.

The Mn^{2+} variation induced by geochemical reaction shift ranges from -18.2% to 14.59% (Table 2). It should be noted that there are negative values indicating that the geochemical reactions counteract the variation induced by physical mixing. In addition, the variation of Mn^{2+} induced by geochemical reaction is not as significant as Fe^{2+}. In near-surface zone (L2-1 and L3-1), similar to Fe^{2+}, Mn^{2+} variation is very large, but, the net change of Mn^{2+} in near-surface zone (0.034 ~ 0.09 mg/L) is not as large as the transition zone with a salinity of 0.5 ~ 10. In the transition zone with a salinity of 0.5 ~ 10, Mn^{2+} variation is -12.87% ~ 14.59% with a net change of 0.044 ~ 0.115 mg/L. According to Eq. (2), the abiotic oxidation rates of Mn^{2+} in this zone range from 3.3×10^{-8} μM/h to 3.9×10^{-7} μM/h. Such a slow abiotic oxidation rate of Mn^{2+} in this zone cannot cause such a net change of Mn^{2+} (0.044 ~ 0.115 mg/L) in such a short time. For example, total Mn^{2+} variation is 0.084 mg/L for L3-4, in which 0.0015 mg/L (1.79%) is caused by geochemical reactions. Applying the largest abiotic oxidation rate of Mn^{2+} (3.9×10^{-7} μM/h), the time to oxidize Mn^{2+} and to cause a net change of 0.0015 mg/L is about 7.86 years that is far beyond the time scale of tidal fluctuation. Therefore, the abiotic oxidation of Mn^{2+} is not the major driver of Mn^{2+} variation in the salinity transition zone. As stated previously, microbial catalyzed oxidation of Mn^{2+} should be a major pathway for fast removal of Mn^{2+} in this study (Tebo et al., 2004). If the time scale of a tidal cycle is assumed, the microbial catalyzed oxidation rate of Mn^{2+} is estimated to be ~ 1.1×10^{-3} μM h^{-1}. Unlike Fe^{2+} variation is highly influenced by the geochemical reaction, the Mn^{2+} variation is mainly affected by physical mixing, indicating its comparatively conservative properties in the intertidal aquifer of this study.

4.3 The apparent production (or removal) rates of Fe and Mn in the salinity transition zone

The apparent reaction (production or removal) rates of Fe and Mn in the salinity transition zone are estimated a standard estuary model and a transient mass balance model, respectively. The two models are independent to each other and offer reliable cross-validated estimates of Fe^{2+} and Mn^{2+} production (or removal) rates. The estimated apparent production (or removal) rates of Fe^{2+} and Mn^{2+} assists to accurately evaluate the function of salinity transition zone when groundwater borne iron and manganese transports to the ocean.

4.3.1 The standard estuary model

The apparent production rate of Fe^{2+} in the transition zone can be calculated by applying a standard estuarine model, which is described as (Liu et al., 2017a; Santos et al., 2009; Santos et al., 2011),

$$R = \frac{1}{t}\int_{S=0}^{S=25}(C_{bf} - C_{cm})\,dS, \quad (3)$$

where *R* is the production or removal rate of the element, *t* is the time for water flow through the transition zone, *S* is the salinity, C_{bf} and C_{cm} are the concentrations of the element according to the best fit of the data and conservative mixing between the FGW and seawater endmember, respectively. The time for groundwater flowing through the salinity transition zone is estimated by using the lateral width of the zone to divide flow velocity. The hydraulic gradient is calculated to be ~ 0.04 in the upper several meters of the aquifer and the hydraulic conductivity is measured to be 4.79 m/d (Liu et al., 2018a).The flow velocity is calculated to be 0.19 m/d according to Darcy's Law. The lateral width of the salinity transition zone is 20 m. The time for groundwater to flow through the salinity transition zone is estimated to be 104 days. Applying Eq. (3), the apparent production rate of Fe^{2+} and Mn^{2+} in the salinity transition zone is calculated to be 0.37 mg/L/d (or 6.68 μM/d) 0.022 mg/L/d (or 0.4 μM/d), respectively. The apparent production rate of Mn^{2+} is about 6% that of Fe^{2+} demonstrating that the biogeochemical reactions of Mn in the salinity transition zone are not as intensive as Fe. Mn is less active than Fe in the salinity transition zone probably because Mn in solid phase is much lower than Fe in solid phase as observed in sediment core 1 (Figure 6 & Table S2).

4.3.2 The transient mass balance model

The transient apparent production (or removal) rate is defined as the inventory change rate of Fe^{2+} and Mn^{2+} in the salinity transition zone. This transient rate is used to quantify the capacity of an aquifer to produce (or remove) trace metals from the dissolved phase. To calculate the transient apparent production (or removal) rates of Mn and Fe, a model considering the mass balance of both water and solute is applied. The schematic diagram of the mass balance model is presented in Figure 9a and the mathematical expression is shown below,

$$\Delta S = (F_{in} + F_{sw} - F_{out})\Delta t, \quad (4)$$

$$\Delta M = (R + F_{in}C_{in} + F_{sw}C_{sw} - F_{out}C_{out})\Delta t, \quad (5)$$

where ΔS is the water storage variation, which can be calculated according to the groundwater level data at D2, F_{in} is the water influx from the inland boundary, F_{sw} is the recharge of seawater, if the tidal level does not submerge the beach surface of L2 and L3, this term equals 0, F_{out} is the water flux flowing out the region, ΔM is the solute storage change, C_{in} is the solute concentration of fresh groundwater from inland boundary, C_{sw} is the solute concentration of seawater, C_{out} is the solute concentration of saline groundwater seeping out from the domain, *R* is the production or removal rate of the solute from the groundwater. The Eq. (5) can be rewritten as:

$$R = \Delta M/\Delta t + F_{ou} \quad C_{out} - F_{in}C_{in} - F_{sw}C_{sw} \quad , \tag{6}$$

In Eq. (6), the ΔM can be calculated according to the observed data via:

$$\Delta M = M_{i+1} - M_i, \tag{7}$$

where M_i is the total solute mass in the sampling round i. The M_i can be calculated through integrating concentration of a specific element in the domain.

$$M_i = \int nC_i dxdz, \tag{8}$$

where n is the porosity, x and z are the horizontal and vertical coordinates, respectively.

The inventory of Fe^{2+} (total solute mass, *M*, in Eq. (8)) varies obviously with tidal fluctuation. The Mn^{2+} inventory, however, changes much less with tidal fluctuation (Figure 9b). This demonstrates that Mn^{2+} is less active than Fe^{2+} in the salinity transition zone. Roughly, Fe^{2+} inventory in the salinity transition zone is larger during low tide than during high tide, which is because the inland water flux enriched in Fe^{2+} and Mn^{2+} is larger at low tide than at high tide. The transient production (or removal) rate of Fe has a much larger fluctuation than that of Mn (Figure 9c). More importantly, while Fe is removed from dissolved phase (negative value) the dissolved Mn is produced (positive value), which demonstrates the competition between the Fe^{2+} and Mn^{2+} serving as the electron receiver in geochemical reactions as stated previously. It is worth noting that the decrease of reaction rate lasts longer time than the decrease of tidal level. This is because seaward flow dominates during a tidal cycle, brings a large amount of Fe^{2+} from inland area, and hinders the production of Fe^{2+} in the salinity transition zone. Nevertheless, at high tide, the decrease of inland flux with high Fe^{2+} and also the landward movement of high salinity water enriched in reducers like H_2S facilitates the reductive dissolution of iron oxides in the salinity transition zone and results in a high production rate of Fe^{2+} during high tidal. During the whole sampling period, the apparent production rate of Fe^{2+} and Mn^{2+} in the salinity transition zone is 0.27 mg/L/d and 0.04 mg/L/d, respectively (Figure 9d). The estimates using the mass balance model are very close to that calculated via the standard estuary model (0.27 vs. 0.37 mg/L/d for Fe^{2+} and 0.04 vs 0.022 mg/L/d for Mn^{2+}). The very small production rate (close to zero) of Mn^{2+} suggests the inactive properties of Mn in the salinity transition zone of this study.

4.4 Biogeochemistry of trace metals in the salinity transition zone

Many studies have demonstrated the oxidation of groundwater borne ferrous iron and precipitation of iron (hydr)oxides in the salinity transition zone (Charette and Sholkovitz, 2002; Charette et al., 2005; McAllister et al., 2015). It could be expected that there are many iron (hydro)oxides precipitated in the freshwater front of transition zone in this study. The increase of Fe in solid phase below 67.5 cm at L2 (core1) is a piece of evidence of the precipitation of Fe^{2+} along with the fresh groundwater advection. In addition, a large amount of iron (hydro)oxides are found in the sediments below 67.5 cm (core 1) and 50 cm (core 2) based on SEM images (Figure 10). Therefore, the enrichment of Fe^{2+} in groundwater with salinity < 5 is attributed to the reductive dissolution of iron (hydro)oxides in the aquifer (Figure 7a). During the reductive dissolution of iron (hydro)oxides, the organic matters from infiltrated NSW and hydrogen sulfide (H_2S) from sulfate (SO_4^{2-}) reduction would serve as the electron suppliers. Owing to a very quick variation of Fe^{2+} in response to tidal fluctuation (Figures 4 & 9), a fast dissolution of iron oxides is required. Among the four parallel pathways with different dissolution rates (proto-promoted, ligand-promoted, reductive, and synergistic), reductive and synergistic dissolutions are the two fastest form of dissolution (Hyacinthe et al., 2006; Martin, 2005). The cycling between Fe^{2+} and FeOOH in the salinity transition zone is an important pathway of the geochemical transformations between the Fe in liquid and solid phases, which has been systematically discussed in McAllister et al. (2015) and will not be repeated in this study. In this study, to meet the requirement of quick reductive dissolution within short time scale such as several hours (tidal scale), the amorphous $Fe(OH)_3$ that has a dissolution rate several times faster than other forms of iron oxides such as FeOOH and hematite (Bonneville et al., 2004; Roden, 2003) would be the most possible form of oxidized iron in the salinity transition zone. In addition, a large fraction (> 80%) of amorphous oxides is found to be subject to the bacterial reduction in freshwater sediments (Lovley and Phillips, 1986, 1987; Roden, 2004). The geochemical transformation between Fe^{2+} and amorphous $Fe(OH)_3$ in the salinity transition zone of this study is expressed as:

$$4Fe^{2+} + 3O_2 + 6H_2O \rightarrow 4Fe(OH)_{3(\text{Amorphous})}, \quad (9)$$

$$4Fe(OH)_{3(\text{Amorphous})} + 7CO_2 + [CH_2O] \rightarrow 4Fe^{2+} + 8HCO_3^- + 3H_2O, \quad (10)$$

What should be noted is that the electron accepter in Eq. (9) is not limited to oxygen (O_2) and other electron accepter such as nitrate (NO_3^-) would also function well. In this study, the high Fe^{2+} zone (Figure 4) overlap with the front of NO_3^- plume from deep FGW (Liu et al., 2017c; Liu et al., 2018d). As stated previously, the abiotic reduction of iron

could not meet the fast dissolution of iron oxides. Therefore, the dissimilatory reduction of iron is essential. The iron reducing bacteria such as *shewanella putrefaciens* is known to substitute Fe(III) for O_2 as the terminal electron accepter in respiration as shown in Eq. (10) (DiChristina and DeLong, 1994). These bacteria are commonly in estuarine sediments (Hyacinthe et al., 2006; Lin, 2006). The electron supplier (organic matters) in Eq. (10) could also be replaced by other electron suppliers such as hydrogen sulfide and methane (McAllister et al., 2015).

The decrease of Fe^{2+} in groundwater with salinity > 6 (Figure 7a) is unlikely caused by the Fe removal process described in Eq. (9), because of a much reduced environment (ORP: -80.32 ~ -136.98 mV) (Table 2). In addition, microbial communities in the intertidal aquifer are found to be more enriched in sulfate-reducers than Fe (II)-oxidizers (McAllister et al., 2015). Therefore, the cycling of Fe in this zone (salinity > 6) is expected to be resulted from the precipitation and dissolution of pyrite (FeS_2) or sulfide iron (FeS) minerals. However, the formation of pyrite is very strict and would include a transform of solid monosulfide (FeS) to FeS_2 (Schieber, 2011). Even though H_2S is not measured in this study, the production of H_2S via the sulfate reduction is demonstrated by a very good relationship between removed sulfate and produced total alkalinity at the study site (Liu et al., 2017b). In addition, a large amount of sulfide iron minerals (Figure 11) discovered in sediments of core 2. Therefore, the transformation between Fe^{2+} and sulfide iron is the most possible Fe cycle pathway. The transformation of Fe(II) in liquid phase (Fe^{2+}) to Fe(II) in solid phase (FeS) can be expressed as,

$$Fe^{2+} + H_2S \rightarrow FeS + 2H^+, \quad (11)$$

$$2FeS + 3O_2 + 2H_2O \rightarrow 2Fe^{2+} + 2{SO_4}^{2-} + 4H^+, \quad (12)$$

The cycling of iron between solid and liquid phase described in Eqs. (11) & (12) is sensitive to the variation of iron concentration, salinity and oxygen concentrations induced by tidal fluctuation because these factors are significantly correlated to the microbial community structure in the intertidal aquifer (McAllister et al., 2015). The electron accepter (O_2) described in Eq. (12) can be replaced by other electron accepter such as nitrate (NO_3^-), especially in the zone (L3-3 and L3-4) where deep FGW meets the saline groundwater due to a high NO_3^- in deep FGW as shown in Liu et al. (2017c).

As for manganese, to meet the requirement of quick transformation between the solid phase and liquid phase, the quickest oxidation and dissolution process can be expressed as (Martin, 2005),

$$4Mn^{2+} + O_2 + 6H_2O \rightarrow 4\,MnOOH_{(s)} + 8H^+, \quad (13)$$

$$4MnOOH_{(s)} + [CH_2O] + 3H^+ \rightarrow 4Mn^{2+} + 3HCO_3^-, \quad (14)$$

The reaction expressed in Eqs. (13) & (14) should be catalyzed by microbial activities since abiotic oxidation of Mn^{2+} and reduction of Mn minerals are too slow to meet the quick variation of Mn^{2+} in groundwater within a tidal cycle (24 h). Since there is very limited content of Mn in dissolved and solid phase at the study site and very small apparent production rate of Mn^{2+} (close to zero) in the salinity transition zone, it can be expected that the Mn cycle described in Eqs. (13) & (14) is not active.

4.5 Conceptual model of trace metals cycling in the intertidal aquifer

Based on the analysis of spatial distribution and biogeochemistry of trace metals in the salinity transition zone, a conceptual model describing the cycling of Mn and Fe in the intertidal aquifer of this study is proposed (Figure 12). Firstly, the shallow FGW brings a large amount of Mn^{2+} and Fe^{2+} to the salinity transition zone. Due to the comparatively rapid transport in the aquifer, the shallow FGW is enriched in DO and characterized by low pH induced by the infiltration acidic rainfall water. Secondly, DO in deep FGW is consumed by abiotic or microbially mediated reactions such as remineralization of organic matter during the transport in the aquifer. Meanwhile, carbon dioxide produced during the remineralization lowers the pH of deep FGW. In addition, the oxidation of Fe and Mn reduces DO, Mn^{2+}, and Fe^{2+} in deep FGW. Other process such as nitrification could also be responsible for a low DO observed in deep FGW. When FGW mixes with NSW (high pH), the increase of pH and residence time accelerates the abiotic oxidation of Fe^{2+} and the oxidation of Mn^{2+} would also facilitated by the unique and abundant microbial communities in the mixing zone. Therefore, the formation of high valence Fe(III) and Mn(III, or IV) and precipitation of oxides occur in the salinity transition zone (Charette and Sholkovitz, 2002, 2006; Charette et al., 2005). Along with the accumulation of Fe and Mn oxides, the reducers such as organic matters, H_2S, methane induced by other processes reacts with the oxides (Fe and Mn) and produces dissolved phases of Fe and Mn. The microbial communities play a significant role in reducing these low soluble iron and manganese oxides. Furthermore, high Fe^{2+} in the salinity transition zone promotes the reaction between Fe^{2+} and H_2S to form FeS minerals, especially in the reduced environment with abundant microbial sulfate-reducers (McAllister et al., 2015). The FeS may precipitate in the aquifer and further to react with H_2S to form a more stable mineral pyrite (FeS_2). However, if the electron accepter is induced to this zone, the dissolution of FeS or pyrite occurs and Fe^{2+} is released. When Fe^{2+}

transport to high salinity zone of the aquifer, the oxidation rate of Fe^{2+} will accelerate drastically with the increase of pH and a large amount of Fe^{2+} will precipitate in a form of Fe oxides eventually if the aquifer is in oxic condition. If the aquifer is in reduced condition, FeS would be another form of iron precipitation. Therefore, although the geochemical transformation of Fe in the salinity transition zone of intertidal aquifer is active, the high salinity zone of intertidal aquifer acts as the sink of Fe^{2+} and only a part of Fe^{2+} will discharge to the sea associated with SGD. This can be demonstrated by the increase of solid phase of Fe observed at core 2 that is collected in the high salinity zone of intertidal aquifer. This is consistent to the findings of previous studies (Charette and Sholkovitz, 2002; Spiteri et al., 2006), however, the removal of Fe^{2+} in the high salinity zone of intertidal aquifer is not necessarily limited to the oxidation of Fe^{2+} as indicated by these studies (Charette and Sholkovitz, 2002; Spiteri et al., 2006), but the precipitation of Fe^{2+} as iron sulfide and pyrite is an alternative pathway (McAllister et al., 2015). Due to the high Fe^{2+}, the geochemical transformation of Mn^{2+} in the salinity transition zone is hindered and Mn^{2+} behaves less active than Fe^{2+} in this study. Therefore, most of the fresh groundwater borne Mn^{2+} discharges to the ocean associated SGD and some of them will precipitate as Mn minerals in the aquifer since an increased solid phase of Mn is observed at core 2. Due to the high Mn^{2+} and very high Fe^{2+} in fresh groundwater, the SGD associated Fe and Mn flux to Tolo Harbor is expected to be large.

5 Conclusion

Through intensive sampling and analysis of trace metals (Fe, Mn, and Sr) in the salinity transition zone of intertidal aquifer of Tolo Harbor at different tidal stages, the dynamics of Fe^{2+}, Mn^{2+}, and Sr^{2+} are presented. The variations of Fe^{2+}, Mn^{2+}, and Sr^{2+} in near-surface zone are affected by physical mixing with infiltrated NSW. Biogeochemical reactions in the salinity transition zone are influenced by tidal fluctuation induced redox condition shift. Fe is the most active while Sr is the most conservative among the three elements. Generally, Sr^{2+} shows a comparatively conservative behavior in the salinity transition zone of intertidal aquifer. Therefore, a simultaneous variation between Sr^{2+} and salinity at different tidal stages is observed. However, Sr^{2+} is removed from groundwater by adsorption to iron oxides in the salinity transition zone. The quick response of biogeochemical reactions involving Fe and Mn to the tidal fluctuation indicates that the pathways of Fe and Mn cycling tend to be biogeochemical reactions with very quick reaction rates. The transformation between amorphous $Fe(OH)_3$ and Fe^{2+} or Fe^{2+} and FeS are responsible for the enrichment of Fe^{2+} in the transition zone with a salinity of 0.5 ~ 10. The production of Fe^{2+} is

found in the salinity transition zone of intertidal aquifer (20 m wide) with a rate of about 0.37 mg/L/d via a standard estuary model and 0.27 mg/L/d via a transient mass balance model. However, only a small proportion of Fe^{2+} discharges to the sea associated with SGD due to the precipitation of Fe in the high salinity zone of intertidal aquifer. The proposed conceptual model generalized the biogeochemical reactions in the intertidal aquifer provides a better understanding of the spatial distribution and biogeochemical transformations of trace metals in the intertidal aquifer. This study suggests that Fe^{2+} will precipitate in the coastal aquifer as a form of Fe oxides or FeS minerals during the transport from land to sea and only a small part of Fe^{2+} discharges to the sea associated with SGD.

Acknowledgements

This study was supported by Seed Fund for Basic Research from the University of Hong Kong. And the work described in this paper (or the equipment/ facility) was partially supported by a grant from the Research Grants Council of the Hong Kong Special Administrative Region, China (Project No. C6001-14G) to Prof Jiao and the Hung Hing Ying Physical Sciences Research Fund (#203730747) of the University of Hong Kong to Dr Not. The authors would like to thank the technicians Mr. Ho, and Dr. Chio for their help of installation of sampler and the field works. The assistances of Mr. Feng and Mr. Cheng when sampling in the field are also appreciated. The authors would like to appreciate Dr. Li for their help in measurement of trace metals in sediments.

References

Andersson, P.S., Wasserburg, G.J., Ingri, J. and Stordal, M.C. (1994) Strontium, Dissolved and Particulate Loads in Fresh and Brackish Waters - the Baltic Sea and Mississippi Delta. Earth and Planetary Science Letters 124, 195-210.

Atkinson, C.A., Jolley, D.F. and Simpson, S.L. (2007) Effect of overlying water pH, dissolved oxygen, salinity and sediment disturbances on metal release and sequestration from metal contaminated marine sediments. Chemosphere 69, 1428-1437.

Beck, A.J., Charette, M.A., Cochran, J.K., Gonneea, M.E. and Peucker-Ehrenbrink, B. (2013) Dissolved strontium in the subterranean estuary - Implications for the marine strontium isotope budget. Geochimica Et Cosmochimica Acta 117, 33-52.

Beck, A.J., Cochran, J.K. and Sanudo-Wilhelmy, S.A. (2009) Temporal Trends of Dissolved Trace Metals in Jamaica Bay, NY: Importance of Wastewater Input and Submarine Groundwater Discharge in an Urban Estuary. Estuaries and Coasts 32, 535-550.

Beck, A.J., Cochran, J.K. and Sanudo-Wilhelmy, S.A. (2010) The distribution and speciation of dissolved trace metals in a shallow subterranean estuary. Marine Chemistry 121, 145-156.

Beck, A.J., Tsukamoto, Y., Tovar-Sanchez, A., Huerta-Diaz, M., Bokuniewicz, H.J. and Sanudo-Wilhelmy, S.A. (2007) Importance of geochemical transformations in determining submarine groundwater discharge-derived trace metal and nutrient fluxes. Applied Geochemistry 22, 477-490.

Beck, M., Dellwig, L., Schnetger, B. and Brumsack, H.J. (2008) Cycling of trace metals (Mn, Fe, Mo, U, V, Cr) in deep pore waters of intertidal flat sediments. Geochimica Et Cosmochimica Acta 72, 2822-2840.

Bone, S.E., Gonneea, M.E. and Charette, M.A. (2006) Geochemical cycling of arsenic in a coastal aquifer. Environmental Science & Technology 40, 3273-3278.

Bonneville, S., Van Cappellen, P. and Behrends, T. (2004) Microbial reduction of iron(III) oxyhydroxides: effects of mineral solubility and availability. Chemical Geology 212, 255-268.

Charette, M.A. and Sholkovitz, E.R. (2002) Oxidative precipitation of groundwater-derived ferrous iron in the subterranean estuary of a coastal bay. Geophysical Research Letters 29, 85-81-85-84.

Charette, M.A. and Sholkovitz, E.R. (2006) Trace element cycling in a subterranean estuary: Part 2. Geochemistry of the pore water. Geochimica Et Cosmochimica Acta 70, 811-826.

Charette, M.A., Sholkovitz, E.R. and Hansel, C.M. (2005) Trace element cycling in a subterranean estuary: Part 1. Geochemistry of the permeable sediments. Geochimica Et Cosmochimica Acta 69, 2095-2109.

DiChristina, T.J. and DeLong, E.F. (1994) Isolation of anaerobic respiratory mutants of Shewannella putrefaciens and genetic analysis of mutants deficient in anaerobic growth on Fe3+. Journal of Bacteriology 176, 1468-1474.

Dulaiova, H., Ardelan, M.V., Henderson, P.B. and Charette, M.A. (2009) Shelf-derived iron inputs drive biological productivity in the southern Drake Passage. Global Biogeochemical Cycles 23.

Fang, M., Lau, P.-s., Wong, H.-L., Tam, A., To, K.-L., Krewitt, W., Heck, T. and Droste-Franke, B. (2001) Study of acid rain in Hong Kong: final report submitted for the provision of service to the Environmental Protection Department, HKSAR (Tender Ref AS 99-417).

Fetter, C.W. (2000) Applied hydrogeology. Prentice hall.

Gonneea, M.E., Charette, M.A., Liu, Q., Herrera-Silveira, J.A. and Morales-Ojeda, S.M. (2014) Trace element geochemistry of groundwater in a karst subterranean estuary (Yucatan Peninsula, Mexico). Geochimica Et Cosmochimica Acta 132, 31-49.

Hatje, V., Payne, T.E., Hill, D.M., McOrist, G., Birch, G.F. and Szymczak, R. (2003) Kinetics of trace element uptake and release by particles in estuarine waters: effects of pH, salinity, and particle loading. Environment International 29, 619-629.

Heiss, J.W. and Michael, H.A. (2014) Saltwater-freshwater mixing dynamics in a sandy beach aquifer over tidal, spring-neap, and seasonal cycles. Water Resources Research 50, 6747-6766.

Heiss, J.W., Post, V.E.A., Laattoe, T., Russoniello, C.J. and Michael, H.A. (2017) Physical Controls on Biogeochemical Processes in Intertidal Zones of Beach Aquifers. Water Resources Research 53, 9225-9244.

Holloway, C.J., Santos, I.R., Tait, D.R., Sanders, C.J., Rose, A.L., Schnetger, B., Brumsack, H.-J., Macklin, P.A., Sippo, J.Z. and Maher, D.T. (2016) Manganese and iron release from mangrove porewaters: A significant component of oceanic budgets? Marine Chemistry 184, 43-52.

Hyacinthe, C., Bonneville, S. and Van Cappellen, P. (2006) Reactive iron(III) in sediments: Chemical versus microbial extractions. Geochimica Et Cosmochimica Acta 70, 4166-4180.

Hylander, L.D., Meili, M., Oliveira, L.J., de Castro e Silva, E., Guimaraes, J.R., Araujo, D.M., Neves, R.P., Stachiw, R., Barros, A.J. and Silva, G.D. (2000) Relationship of mercury with aluminum, iron and manganese oxy-hydroxides in sediments from the Alto Pantanal, Brazil. Science of the Total Environment 260, 97-107.

Johannesson, K.H., Chevis, D.A., Burdige, D.J., Cable, J.E., Martin, J.B. and Roy, M. (2011) Submarine groundwater discharge is an important net source of light and middle REEs to coastal waters of the Indian River Lagoon, Florida, USA. Geochimica Et Cosmochimica Acta 75, 825-843.

Kroeger, K.D., Swarzenski, P.W., Greenwood, W.J. and Reich, C. (2007) Submarine groundwater discharge to Tampa Bay: Nutrient fluxes and biogeochemistry of the coastal aquifer. Marine Chemistry 104, 85-97.

Lee, C.M., Jiao, J.J., Luo, X. and Moore, W.S. (2012) Estimation of submarine groundwater discharge and associated nutrient fluxes in Tolo Harbour, Hong Kong. Science of the Total Environment 433, 427-433.

Lin, B. (2006) Composition and functioning of iron-reducing communities in two contrasting environments, ie a landfill leachate-polluted aquifer and estuarine sediments.

Liu, Q., Charette, M.A., Henderson, P.B., McCorkle, D.C., Martin, W. and Dai, M.H. (2014) Effect of submarine groundwater discharge on the coastal ocean inorganic carbon cycle. Limnology and Oceanography 59, 1529-1554.

Liu, Y. (2017) Geochemical processes and solute transport in coastal groundwater mixing zone. Ph. D Thesis, The University of Hong Kong.

Liu, Y., Jiao, J.J. and Cheng, H.K. (2018a) Tracing submarine groundwater discharge flux in Tolo Harbor, Hong Kong (China). Hydrogeol J 26, 1857-1873.

Liu, Y., Jiao, J.J. and Liang, W. (2017a) Tidal Fluctuation Influenced Physicochemical Parameter Dynamics in Coastal Groundwater Mixing Zone. Estuaries and Coasts, 1-14.

Liu, Y., Jiao, J.J. and Liang, W. (2018b) Tidal Fluctuation Influenced Physicochemical Parameter Dynamics in Coastal Groundwater Mixing Zone. Estuaries and Coasts 41, 988-1001.

Liu, Y., Jiao, J.J., Liang, W. and Kuang, X. (2017b) Hydrogeochemical characteristics in coastal groundwater mixing zone. Applied Geochemistry 85, 49-60.

Liu, Y., Jiao, J.J., Liang, W. and Luo, X. (2017c) Tidal Pumping-Induced Nutrients Dynamics and Biogeochemical Implications in an Intertidal Aquifer. J Geophys Res-Biogeo 122, 3322-3342.

Liu, Y., Jiao, J.J., Liang, W. and Luo, X. (2018c) Using Tidal Fluctuation-Induced Dynamics of Radium Isotopes (224Ra, 223Ra, and 228Ra) to Trace the Hydrodynamics and Geochemical Reactions in a Coastal Groundwater Mixing Zone. Water Resources Research 54, 2909-2930.

Liu, Y., Jiao, J.J. and Luo, X. (2016) Effects of inland water level oscillation on groundwater dynamics and land-sourced solute transport in a coastal aquifer. Coastal Engineering 114, 347-360.

Liu, Y., Liang, W. and Jiao, J.J. (2018d) Seasonality of Nutrient Flux and Biogeochemistry in an Intertidal Aquifer. Journal of Geophysical Research: Oceans 123, 6116-6135.

Lovley, D.R. and Phillips, E.J. (1986) Availability of ferric iron for microbial reduction in bottom sediments of the freshwater tidal Potomac River. Applied and Environmental Microbiology 52, 751-757.

Lovley, D.R. and Phillips, E.J. (1987) Competitive mechanisms for inhibition of sulfate reduction and methane production in the zone of ferric iron reduction in sediments. Applied and Environmental Microbiology 53, 2636-2641.

Luo, X. and Jiao, J.J. (2016) Submarine groundwater discharge and nutrient loadings in Tolo Harbor, Hong Kong using multiple geotracer-based models, and their implications of red tide outbreaks. Water Research 102, 11-31.

Luo, X., Jiao, J.J., Moore, W.S. and Lee, C.M. (2014) Submarine groundwater discharge estimation in an urbanized embayment in Hong Kong via short-lived radium isotopes and its implication of nutrient loadings and primary production. Mar Pollut Bull 82, 144-154.

Luo, X., Kwok, K.L., Liu, Y. and Jiao, J. (2017) A Permanent Multilevel Monitoring and Sampling System in the Coastal Groundwater Mixing Zones. Ground Water 55, 577-587.

Martin, S.T. (2005) Precipitation and dissolution of iron and manganese oxides, Environmental Catalysis. CRC Press, pp. 61-82.

McAllister, S.M., Barnett, J.M., Heiss, J.W., Findlay, A.J., MacDonald, D.J., Dow, C.L., Luther, G.W., Michael, H.A. and Chan, C.S. (2015) Dynamic hydrologic and biogeochemical processes drive microbially enhanced iron and sulfur cycling within the intertidal mixing zone of a beach aquifer. Limnology and Oceanography 60, 329-345.

Moore, W.S. (1999) The subterranean estuary: a reaction zone of ground water and sea water. Marine Chemistry 65, 111-125.

Nath, B., Birch, G. and Chaudhuri, P. (2013) Trace metal biogeochemistry in mangrove ecosystems: a comparative assessment of acidified (by acid sulfate soils) and non-acidified sites. Science of the Total Environment 463-464, 667-674.

O'Connor, A.E., Krask, J.L., Canuel, E.A. and Beck, A.J. (2018) Seasonality of major redox constituents in a shallow subterranean estuary. Geochimica et Cosmochimica Acta 224, 344-361.

O'Connor, A.E., Luek, J.L., McIntosh, H. and Beck, A.J. (2015) Geochemistry of redox-sensitive trace elements in a shallow subterranean estuary. Marine Chemistry 172, 70-81.

Parikh, S.J. and Chorover, J. (2005) FTIR spectroscopic study of biogenic Mn-oxide formation by Pseudomonas putida GB-1. Geomicrobiology Journal 22, 207-218.

Porubsky, W.P., Weston, N.B., Moore, W.S., Ruppel, C. and Joye, S.B. (2014) Dynamics of submarine groundwater discharge and associated fluxes of dissolved nutrients, carbon, and trace gases to the coastal zone (Okatee River estuary, South Carolina). Geochimica Et Cosmochimica Acta 131, 81-97.

Rahaman, W. and Singh, S.K. (2012) Sr and 87Sr/86Sr in estuaries of western India: Impact of submarine groundwater discharge. Geochimica et Cosmochimica Acta 85, 275-288.

Robinson, C., Li, L. and Barry, D.A. (2007) Effect of tidal forcing on a subterranean estuary. Advances in Water Resources 30, 851-865.

Rodellas, V., Garcia-Orellana, J., Masque, P., Feldman, M. and Weinstein, Y. (2015) Submarine groundwater discharge as a major source of nutrients to the Mediterranean Sea. Proceedings of the National Academy of Sciences 112, 3926-3930.

Roden, E.E. (2003) Fe(III) Oxide Reactivity Toward Biological versus Chemical Reduction. Environmental Science & Technology 37, 1319-1324.

Roden, E.E. (2004) Analysis of long-term bacterial vs. chemical Fe(III) oxide reduction kinetics1 1Associate editor: P. Maurice. Geochimica et Cosmochimica Acta 68, 3205-3216.

Roy, M., Martin, J.B., Cable, J.E. and Smith, C.G. (2013) Variations of iron flux and organic carbon remineralization in a subterranean estuary caused by inter-annual variations in recharge. Geochimica Et Cosmochimica Acta 103, 301-315.

Roy, M., Martin, J.B., Cherrier, J., Cable, J.E. and Smith, C.G. (2010) Influence of sea level rise on iron diagenesis in an east Florida subterranean estuary. Geochimica Et Cosmochimica Acta 74, 5560-5573.

Roy, M., Martin, J.B., Smith, C.G. and Cable, J.E. (2011) Reactive-transport modeling of iron diagenesis and associated organic carbon remineralization in a Florida (USA) subterranean estuary. Earth and Planetary Science Letters 304, 191-201.

Sanders, C.J., Santos, I.R., Barcellos, R. and Silva Filho, E.V. (2012) Elevated concentrations of dissolved Ba, Fe and Mn in a mangrove subterranean estuary: Consequence of sea level rise? Continental Shelf Research 43, 86-94.

Santos, I.R., Burnett, W.C., Chanton, J., Mwashote, B., Suryaputra, I.G. and Dittmar, T. (2008) Nutrient biogeochemistry in a Gulf of Mexico subterranean estuary and groundwater ‐ derived fluxes to the coastal ocean. Limnology and Oceanography 53, 705-718.

Santos, I.R., Burnett, W.C., Dittmar, T., Suryaputra, I.G.N.A. and Chanton, J. (2009) Tidal pumping drives nutrient and dissolved organic matter dynamics in a Gulf of Mexico subterranean estuary. Geochimica Et Cosmochimica Acta 73, 1325-1339.

Santos, I.R., Burnett, W.C., Misra, S., Suryaputra, I.G.N.A., Chanton, J.P., Dittmar, T., Peterson, R.N. and Swarzenski, P.W. (2011) Uranium and barium cycling in a salt wedge subterranean estuary: The influence of tidal pumping. Chemical Geology 287, 114-123.

Schieber, J. (2011) Iron Sulfide Formation, in: Reitner, J., Thiel, V. (Eds.), Encyclopedia of Geobiology. Springer Netherlands, Dordrecht, pp. 486-502.

Schulz, H.D. and Zabel, M. (2006) Marine geochemistry. Springer.

Shaw, T.J., Gieskes, J.M. and Jahnke, R.A. (1990) Early Diagenesis in Differing Depositional-Environments - the Response of Transition-Metals in Pore Water. Geochimica Et Cosmochimica Acta 54, 1233-1246.

Slomp, C.P. and Van Cappellen, P. (2004) Nutrient inputs to the coastal ocean through submarine groundwater discharge: controls and potential impact. Journal of Hydrology 295, 64-86.

Snyder, M., Taillefert, M. and Ruppel, C. (2004) Redox zonation at the saline-influenced boundaries of a permeable surficial aquifer: effects of physical forcing on the biogeochemical cycling of iron and manganese. Journal of Hydrology 296, 164-178.

Spiteri, C., Regnier, P., Slomp, C.P. and Charette, M.A. (2006) pH-Dependent iron oxide precipitation in a subterranean estuary. Journal of Geochemical Exploration 88, 399-403.

Spiteri, C., Van Cappellen, P. and Regnier, P. (2008) Surface complexation effects on phosphate adsorption to ferric iron oxyhydroxides along pH and salinity gradients in estuaries and coastal aquifers. Geochimica Et Cosmochimica Acta 72, 3431-3445.

Sulu-Gambari, F., Seitaj, D., Behrends, T., Banerjee, D., Meysman, F.J.R. and Slomp, C.P. (2016) Impact of cable bacteria on sedimentary iron and manganese dynamics in a seasonally-hypoxic marine basin. Geochimica Et Cosmochimica Acta 192, 49-69.

Tagliabue, A., Bowie, A.R., Boyd, P.W., Buck, K.N., Johnson, K.S. and Saito, M.A. (2017) The integral role of iron in ocean biogeochemistry. Nature 543, 51-59.

Tebo, B.M., Bargar, J.R., Clement, B.G., Dick, G.J., Murray, K.J., Parker, D., Verity, R. and Webb, S.M. (2004) Biogenic manganese oxides: properties and mechanisms of formation. Annu. Rev. Earth Planet. Sci. 32, 287-328.

Tebo, B.M., Ghiorse, W.C., Van Waasbergen, L.G., Siering, P.L. and Caspi, R. (1997) Bacterially mediated mineral formation; insights into manganese (II) oxidation from molecular genetic and biochemical studies. Reviews in Mineralogy and Geochemistry 35, 225-266.

Tebo, B.M., Johnson, H.A., McCarthy, J.K. and Templeton, A.S. (2005) Geomicrobiology of manganese(II) oxidation. Trends in Microbiology 13, 421-428.

Trezzi, G., Garcia-Orellana, J., Rodellas, V., Masque, P., Garcia-Solsona, E. and Andersson, P.S. (2017) Assessing the role of submarine groundwater discharge as a source of Sr to the Mediterranean Sea. Geochimica Et Cosmochimica Acta 200, 42-54.

Trezzi, G., Garcia-Orellana, J., Rodellas, V., Santos-Echeandia, J., Tovar-Sanchez, A., Garcia-Solsona, E. and Masque, P. (2016) Submarine groundwater discharge: A significant source of dissolved trace metals to the North Western Mediterranean Sea. Marine Chemistry 186, 90-100.

Tse, K.C. and Jiao, J.J. (2008) Estimation of submarine groundwater discharge in Plover Cove, Tolo Harbour, Hong Kong by 222Rn. Marine Chemistry 111, 160-170.

Windom, H.L., Moore, W.S., Niencheski, L.F.H. and Jahrike, R.A. (2006) Submarine groundwater discharge: A large, previously unrecognized source of dissolved iron to the South Atlantic Ocean. Marine Chemistry 102, 252-266.

Xin, P., Robinson, C., Li, L., Barry, D.A. and Bakhtyar, R. (2010) Effects of wave forcing on a subterranean estuary. Water Resources Research 46, W12505.

Table 1. The salinity, pH, DO, ORP, and concentrations of Fe^{2+}, Mn^{2+}, and Sr^{2+} in different water masses.

Concentrations		Shallow FGW	Deep FGW	Saline groundwater	NSW
Salinity (-)	Max	0.26	0.30	21.12	25.94
	Min	0.17	0.22	0.60	23.57
	Average	0.20	0.25	8.40	24.49
pH (-)	Max	7.10	7.04	8.32	8.74
	Min	6.08	5.80	5.71	7.56
	Average	6.58	6.38	6.62	8.21
DO (ppm)	Max	5.86	4.10	5.13	5.90
	Min	2.58	0.33	0.40	2.94
	Average	4.48	2.69	2.80	4.50
ORP (mV)	Max	-10.10	61.60	11.80	-37.50
	Min	-61.50	-52.30	-251.10	-78.80
	Average	-30.50	12.20	-107.70	-55.30
Fe (mg/L)	Max	3.86	1.84	14.43	0.65
	Min	1.83	0.67	0.10	0.04
	Average	3.13	0.98	4.13	0.18
Mn (mg/L)	Max	0.39	0.32	0.63	0.04
	Min	0.17	0.14	0.06	b.d.l.
	Average	0.29	0.25	0.26	b.d.l.
Sr (mg/L)	Max	0.14	0.07	3.30	4.72
	Min	0.05	0.03	0.00	2.03
	Average	0.09	0.05	0.96	3.55

b.d.l. means below detection limit

Table 2. Variation of salinity, pH, ORP, Fe^{2+}, Mn^{2+}, and Sr^{2+} within the tidal cycles during the sampling period.

Water mass	Tubes	Salinity[+]	SD[*]	pH[+]	SD	ORP[+]	SD	Fe^{2+}	SD	Mn^{2+}	SD	Sr^{2+}	SD	Physical mixing induced variation[#]	Geochemical reaction induced variation[^]	
		(-)	(%)	(-)	(%)	(mV)	(%)	(mg/L)	(%)	(mg/L)	(%)	(mg/L)	(%)	Sr (%)	Fe (%)	Mn (%)
Shallow FGW	**L1-2**	0.20	10.55	6.59	4.30	-30.50	46.47	2.93	31.22	0.29	20.56	0.09	24.14	24.14	7.08	-3.58
Saline groundwater	**L2-1**	13.29	24.91	6.62	5.74	-164.95	17.34	1.70	82.40	0.28	32.49	1.56	50.67	50.67	31.73	-18.18
Saline groundwater	**L2-2**	1.67	5.68	6.32	5.43	-47.37	44.78	3.78	47.21	0.34	23.88	0.27	17.43	17.43	29.78	6.45
Saline groundwater	**L2-3**	0.83	11.96	6.32	5.00	-14.32	190.32	5.18	47.07	0.45	25.78	0.16	38.65	38.65	8.42	-12.87
Deep FGW	**L2-4**	0.25	8.91	6.36	6.17	12.19	247.95	0.98	28.62	0.25	20.73	0.05	22.92	22.92	5.7	-2.19
Saline groundwater	**L3-1**	19.91	2.74	6.84	7.69	-233.81	4.88	0.41	65.38	0.14	25.19	2.56	12.27	12.27	53.11	12.92
Saline groundwater	**L3-3**	6.01	9.31	6.73	6.76	-136.82	14.40	5.77	35.89	0.29	19.30	0.59	18.55	18.55	17.34	0.75
Saline groundwater	**L3-4**	5.52	4.59	6.70	6.02	-80.32	21.62	9.69	26.04	0.33	25.30	0.64	23.51	23.51	2.53	1.79
Saline grundwater	**L3-5**	9.03	1.09	6.80	8.23	-81.71	37.24	4.23	31.99	0.11	41.51	1.22	26.92	26.92	5.07	14.59
NSW	**NSW**	24.49	2.64	8.18	3.55	-55.31	22.13	0.18	100.55	-	-	3.55	18.11	18.11	82.44	-

[+] Average value; [*] The standard deviation; [#] the value is the variation of Sr; [^] the value is calculated via total vitiation – physical mixing induced variation

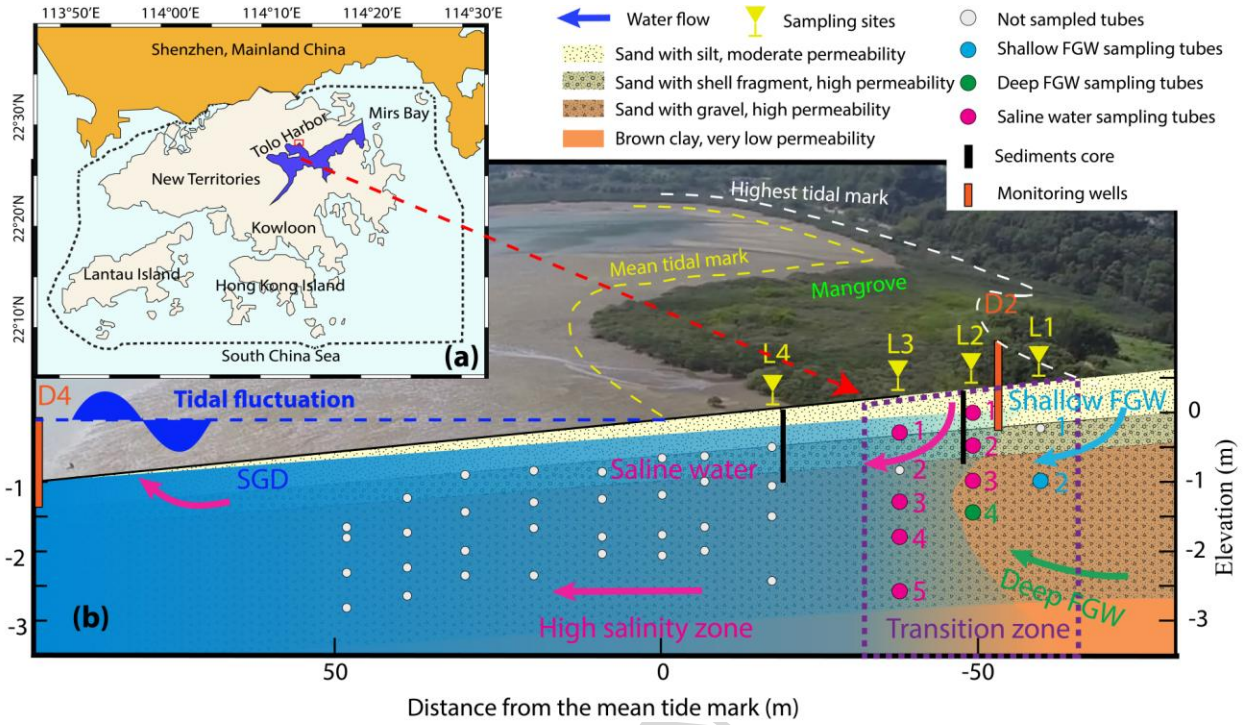

Figure 1. (a) The location of study site at Tolo Harbor, Hong Kong, (b) The vertical placement of the multilevel sampling system and water level monitoring well, the sketch of the water flow and aquifer system, and the location of transition zone. Note, the dots with colored fill in (b) are sampled while the white dots are not sampled in this study, FGW is the abbreviation of fresh groundwater, the shallow and deep FGW is separated according to the stable isotopic composition (δ^2H and $\delta^{18}O$) (Liu et al., 2017c).

Groundwater level at D2 and tidal level at different sampling rounds

SR	01	02	03	04	05	06	07	08	09	10	11	12	13	14	15
Tidal level (m)	-0.81	-1.02	-0.31	0.23	-0.43	0.58	0.8	-0.1	-1.02	-0.44	0.21	-0.49	0.8	0.7	-0.15
D2 (m)	0.48	0.44	0.40	0.36	0.32	0.52	0.72	0.70	0.69	0.69	0.68	0.64	0.77	0.69	0.67

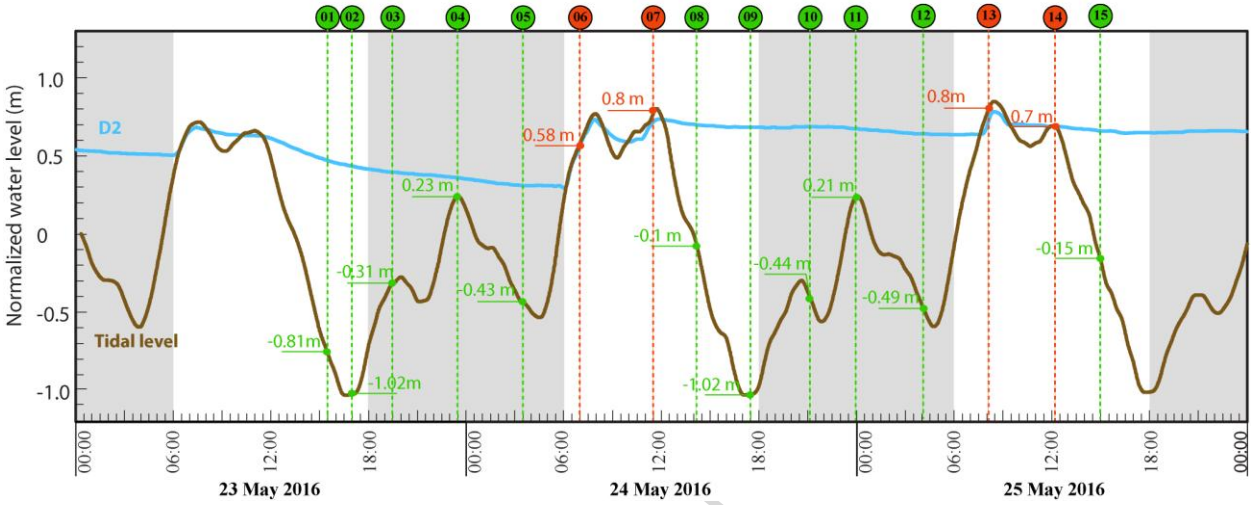

Figure 2. The tidal level (D4 in Figure 1) and groundwater level (D2) fluctuation during the sampling period, the exact time and tidal level at each sampling round (SR), and the surface elevation of sampling sites L1, L2, and L3. The figure is modified from Liu et al. (2017c)

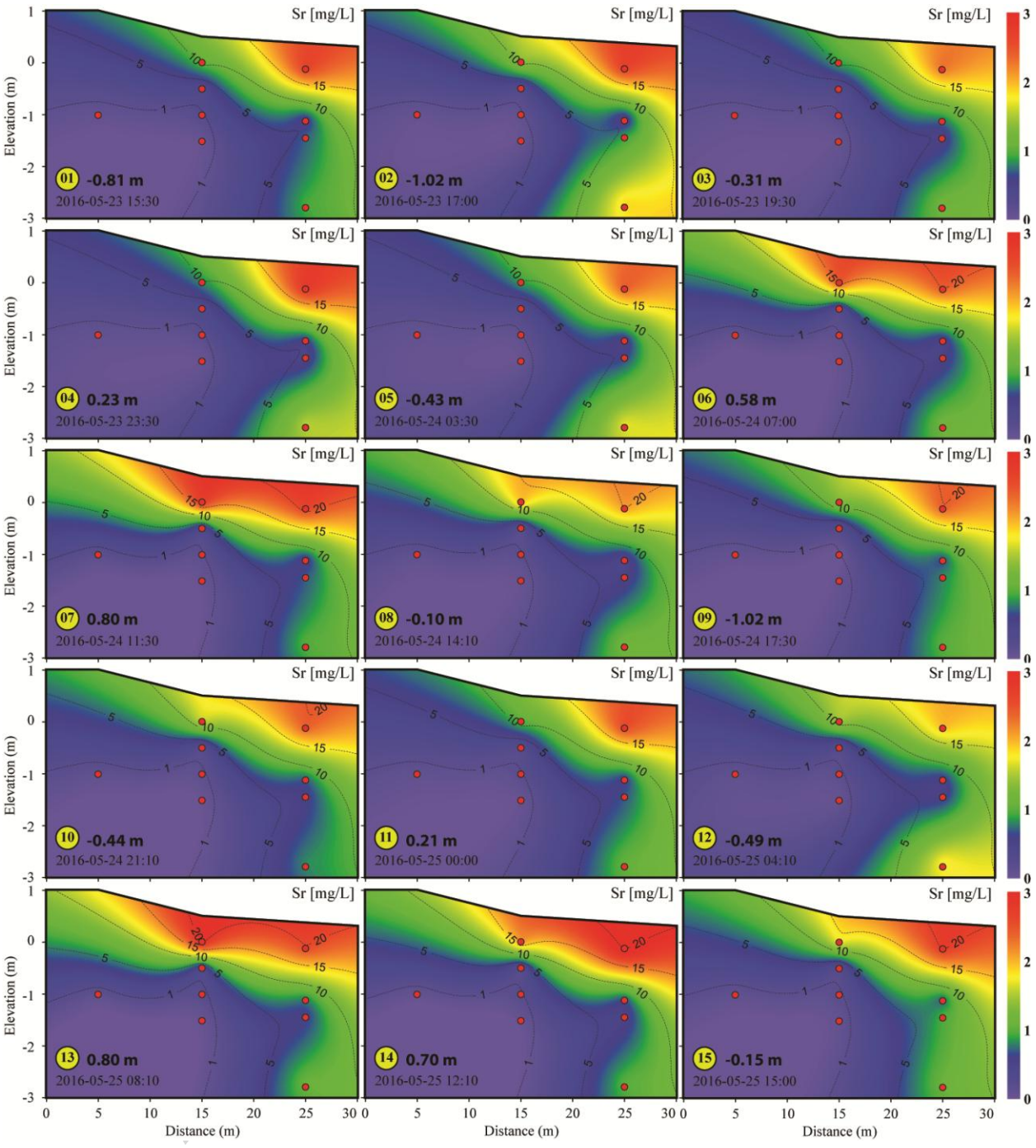

Figure 3. The dynamics of Sr^{2+} (color contour) and salinity (black solid line). The SRs and corresponding sampling time and tidal level are denoted at the bottom left corner.

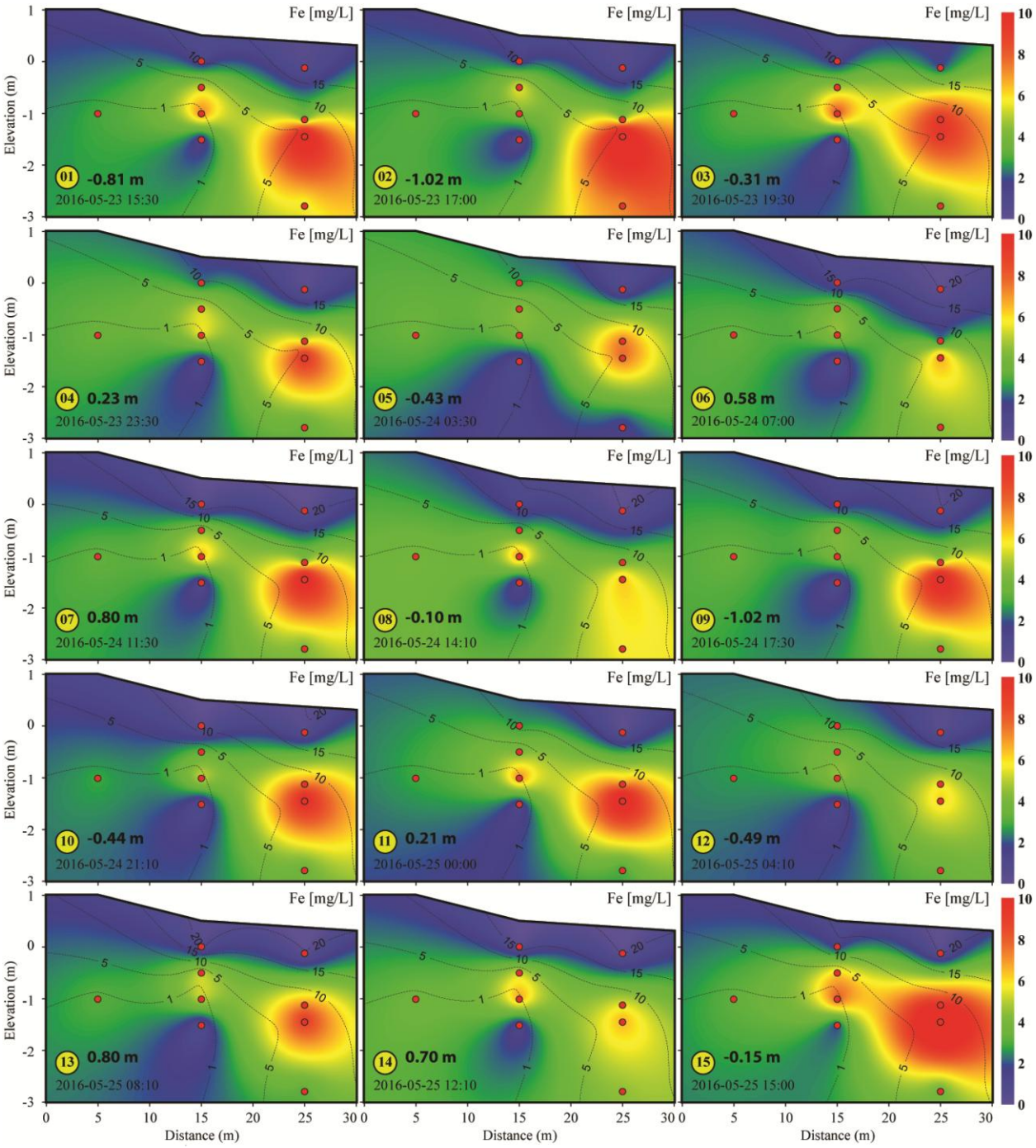

Figure 4. The dynamics of Fe^{2+} (color contour) and salinity (black solid line). The SRs and corresponding sampling time and tidal level are denoted at the bottom left corner.

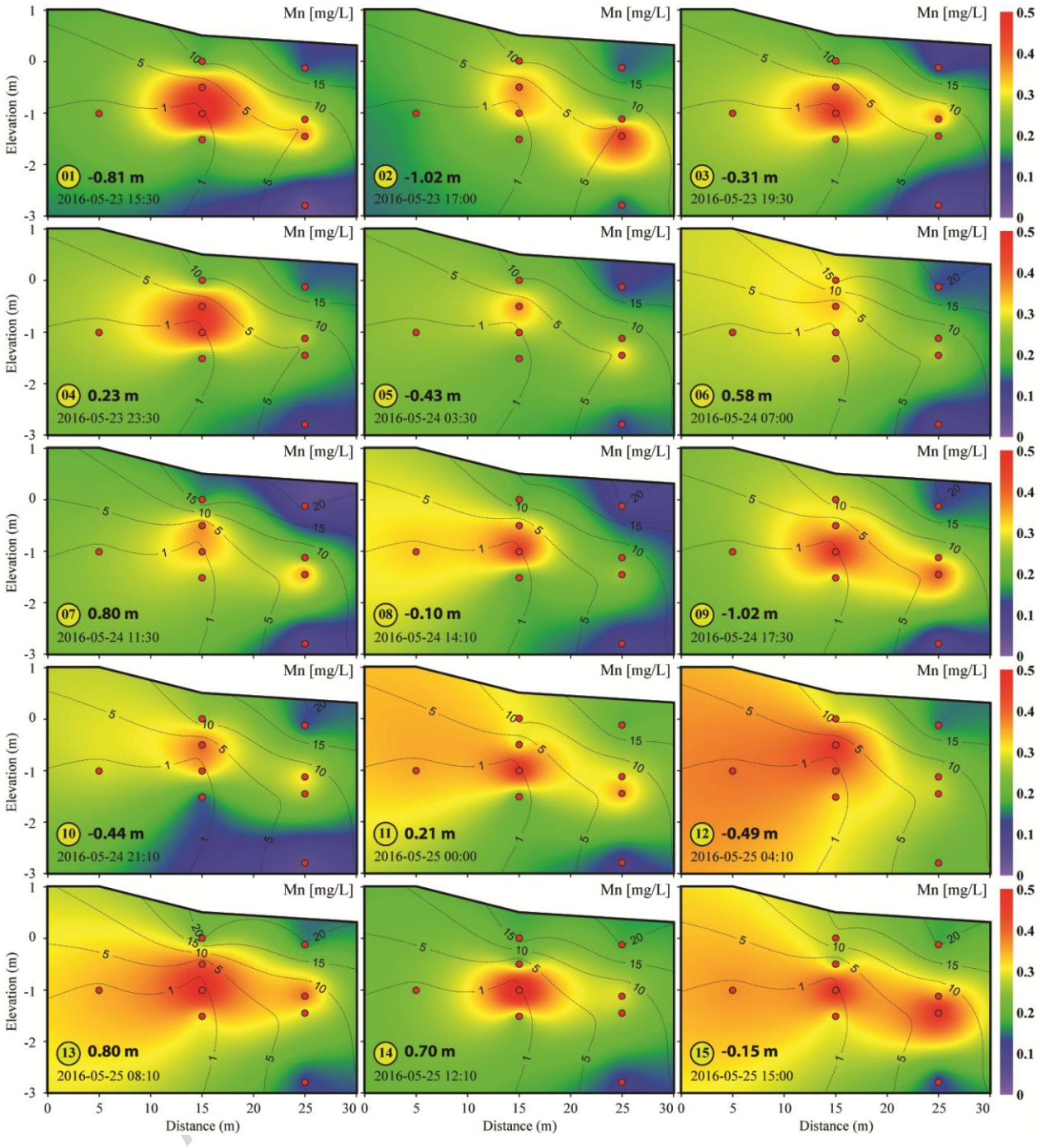

Figure 5. The dynamics of Mn^{2+} (color contour) and salinity (black solid line). The SRs and corresponding sampling time and tidal level are denoted at the bottom left corner

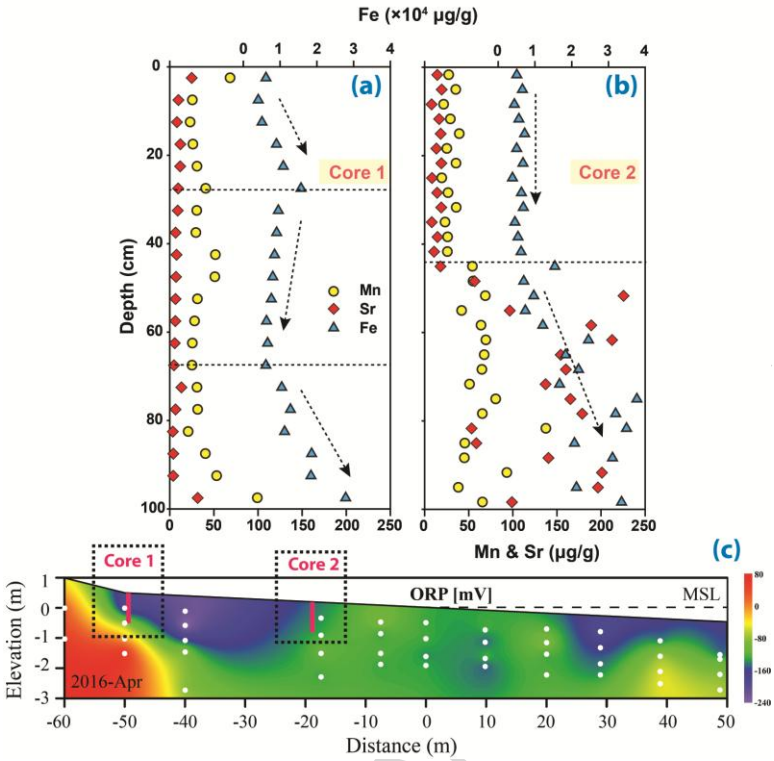

Figure 6. The solid phases of trace metals in (a) core 1and (b) core 2, and (c) the locations of sediment core and corresponding ORP values in April 2016 (Liu et al., 2018d)

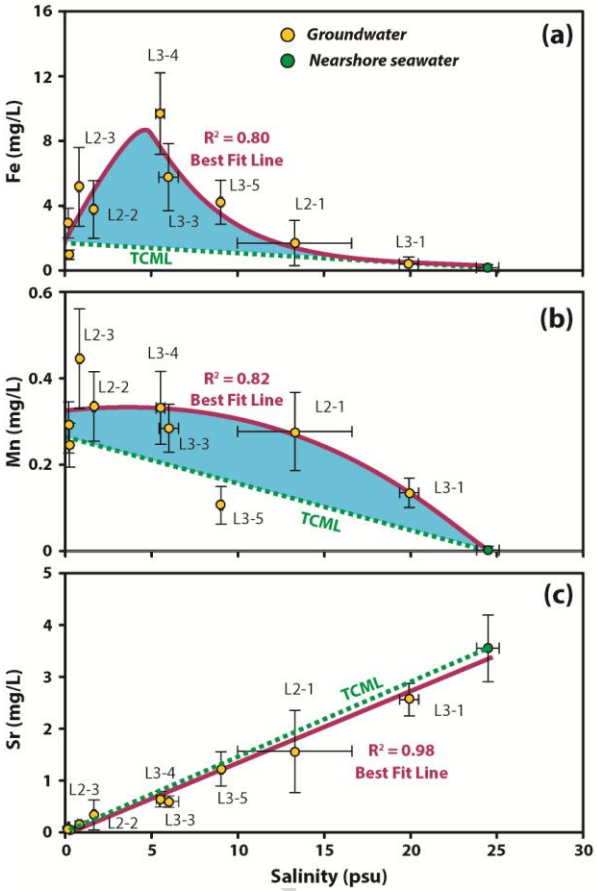

Figure 7. The relationship between salinity and trace metals, (a) Fe^{2+} vs. salinity, (a) Mn^{2+} vs. salinity, (a) Sr^{2+} vs. salinity. The "TCML" denotes the theoretical conservative mixing line, which is made using average concentration of trace metals in shallow and deep FGW.

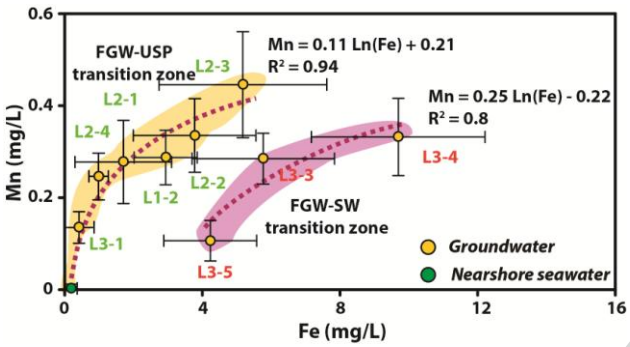

Figure 8. The relationship between Fe^{2+} and Mn^{2+} in FGW-USP transition zone and FGW-SW transition zone. FGW = fresh groundwater, USP = upper saline plume, SW = salt wedge

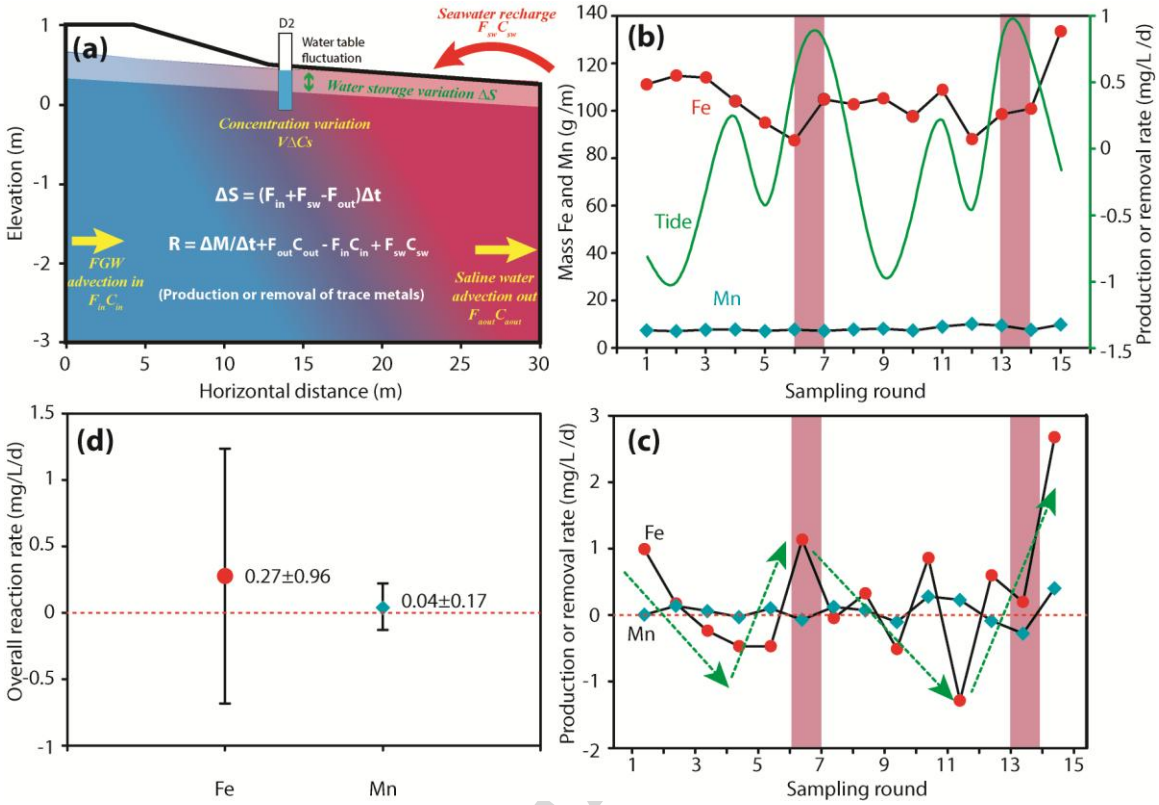

Figure 9. (a) Sketch of the transient mass balance model in salinity transition zone of the intertidal aquifer, (b) the total mass of Fe and Mn in the salinity transition zone and tidal flucutaiton inforamtion, (c) the reactions rates of Fe and Mn in the salinity transition zone at different tidal stages, the positive value represents the production of Fe and Mn while the negative value denotes the removal of Fe and Mn from the saline groundwater in the salinity transition zone, (d) the apparent reaction rates of Fe and Mn in the salinity transition zone, the error bar is the standard deviation during the sampling period. The pink area background in (b) and (c) representes the high tide period denoting the tidal level submerges the ground surface of sampling site L2 and L3.

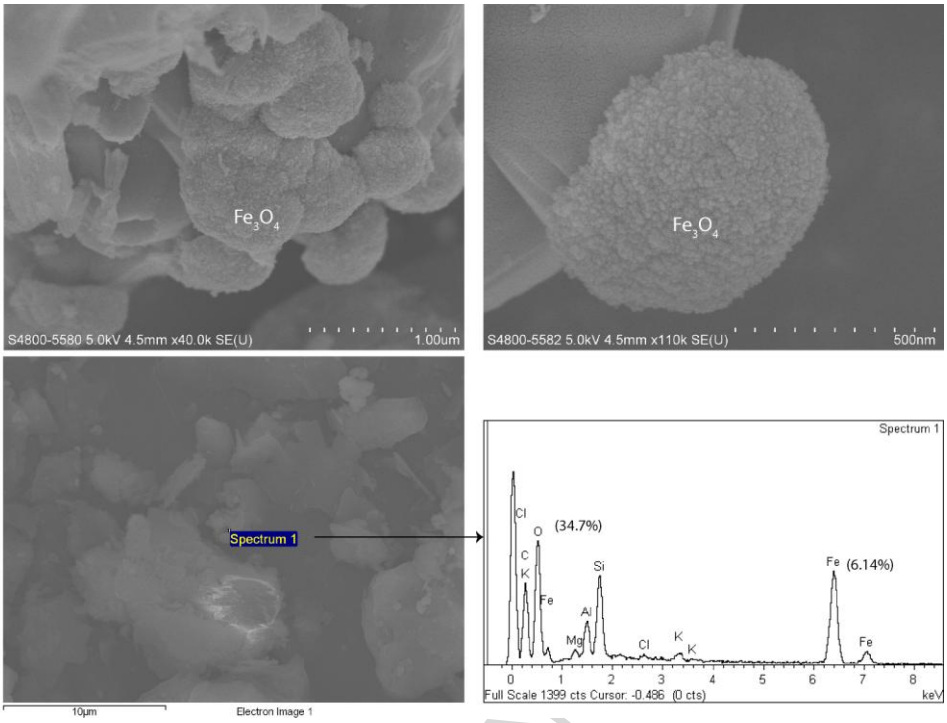

Figure 10. The SEM images of iron (hydro)oxides in sediments 1 m below the beach surface.

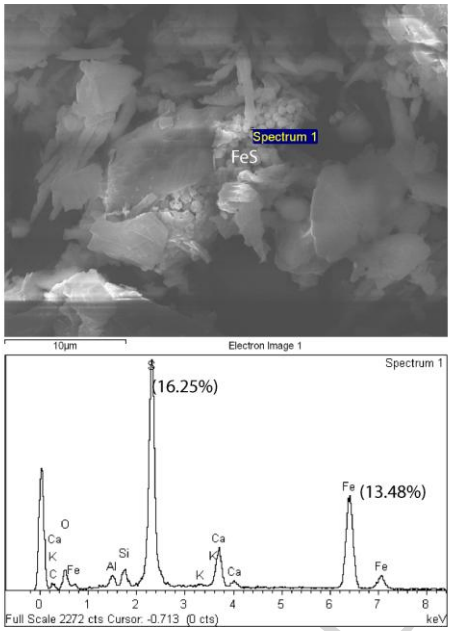

Figure 11. The SEM images of FeS minerals in the sediments

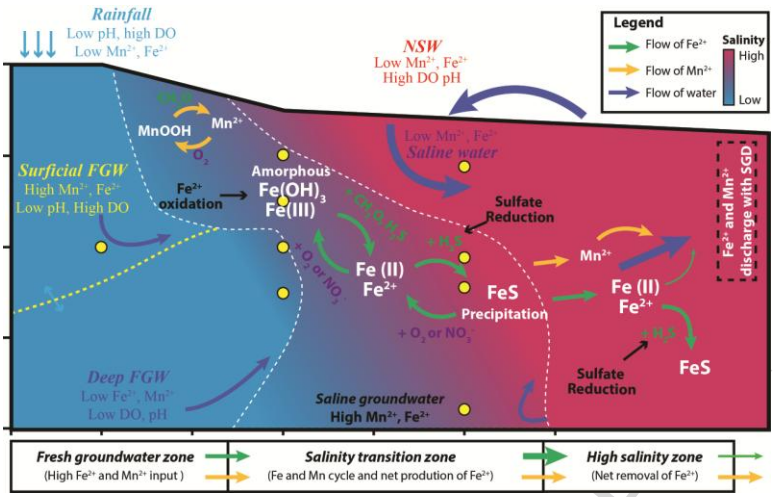

Figure 12. The conceptual model of Fe and Mn cycling in the salinity transition zone of an intertidal aquifer

Author contribution

Conceptualization (Liu & Jiao);

Data curation (Liu, Jiao & Not);

Formal analysis (Liu & Not);

Funding acquisition (Jiao & Not);

Investigation (Liu, Liang & Lu);

Methodology (Liu, Jiao, & Not);

Project administration (Liu, Not & Jiao);

Resources (Jiao & Not);

Supervision (Jiao & Not);

Visualization (Liu);

Roles/Writing - original draft (Liu);

Writing - review & editing (Liu, Not, Jiao, Liang, Lu).

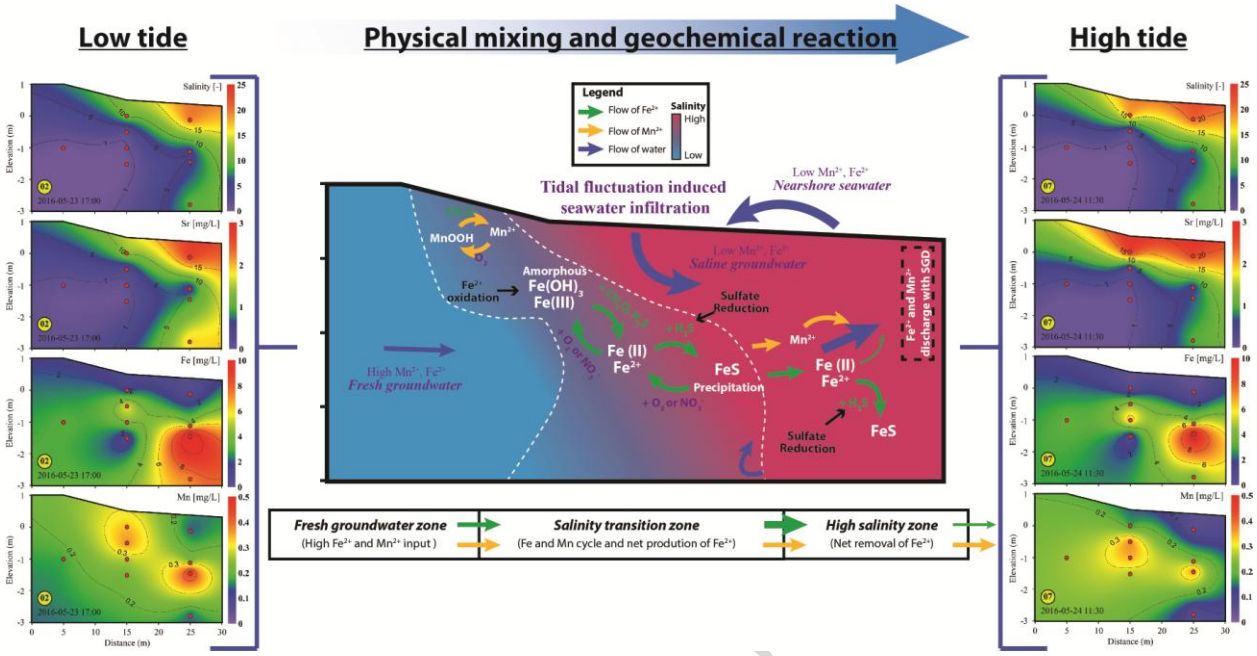

Graphical abstract

Highlights

- Fe^{2+} production at the fresh groundwater front of the salinity transition zone
- Fe removal in a form of FeS mineral in the high salinity zone of an intertidal aquifer
- Tidal induced variation of trace metal geochemistry in an intertidal aquifer
- Clarify multiple pathways of iron cycling in the intertidal aquifer
- Iron cycling in intertidal aquifer affects Fe discharge flux.